Petroleum Science 23 (2026) 7230–7248

Contents lists available at ScienceDirect

Petroleum Science

journal homepage: www.keaipublishing.com/en/journals/petroleum-science

Original Paper

Drilling knowledge constrained deep learning for autonomous drilling optimization in deep geological formations

Zhi-Jun Pei [a,b], Xian-Zhi Song [a,*], Bo Feng [c], Jian He [c], Shou-Ceng Tian [a], Gen-Sheng Li [a]

[a] State Key Laboratory of Petroleum Resources and Prospecting, China University of Petroleum (Beijing), Beijing, 102249, China
[b] State Key Laboratory of Oil & Gas Reservoir Geology and Exploitation, Southwest Petroleum University, Chengdu, 610500, Sichuan, China
[c] CNPC Western Drilling Engineering Co., Ltd., Karamay, 834000, Xinjiang, China

ARTICLE INFO

Article history:
Received 28 October 2025
Received in revised form
24 February 2026
Accepted 14 June 2026
Available online 19 June 2026

Edited by Jia-Jia Fei

Keywords:
Rate of penetration prediction
Physics-informed neural networks
Oil drilling knowledge integration
Intelligent drilling optimization
Constraint-based modeling

ABSTRACT

The development of deep and ultra-deep underground resources is often constrained by high drilling costs and low operational efficiency, among which the rate of penetration (ROP) serving as a critical indicator of drilling performance. Accurate ROP prediction is therefore essential for drilling optimization and cost reduction. However, existing data-driven models typically neglect domain-specific drilling knowledge and physical constraints, leading to poor generalization capability and physically inconsistent predictions, which limits their reliability in practical engineering applications. To address these challenges, this study develops a physically informed and robust ROP prediction framework by integrating drilling knowledge into deep learning models. Based on field data from seven ultra-deep wells in the Tarim Oilfield, China, a drilling knowledge constrained deep neural network (DCDNN) is proposed, in which both soft constraints (correlation relationships among drilling parameters) and hard constraints (boundary condition constraints) are explicitly embedded into the loss function and network structure. This design enhances the physical consistency and robustness of the model, particularly under boundary and extreme operating conditions. Experimental results demonstrate that the proposed DCDNN model improves ROP prediction accuracy by 12.17% compared with conventional neural networks, while maintaining stable performance under constraint conditions. Furthermore, a multi-objective optimization framework is established to simultaneously maximize ROP and minimize bit mechanical specific energy (BMSE). Under simulated optimized drilling parameters, the model projects a 51.09% increase in ROP in the Paleogene Kumugeliemu Formation, indicating strong optimization potential for drilling strategies characterized by high weight on bit and medium rotary speed. The novelty of this work lies in the systematic fusion of drilling mechanism knowledge with deep neural networks through unified soft–hard constraint incorporation, enabling both high prediction accuracy and physical interpretability. Despite the promising results, challenges remain in terms of data completeness, model transferability across different geological settings, and real-time deployment. Future work will focus on extending the proposed framework to multi-block datasets and integrating it into closed-loop intelligent drilling optimization systems.

© 2026 Publishing services by Elsevier B.V. on behalf of KeAi Communications Co. Ltd. This is an open access article under the CC BY-NC-ND license (http://creativecommons.org/licenses/by-nc-nd/4.0/).

1. Introduction

Drilling engineering involves the use of mechanical equipment to break formation rock and create circular boreholes of a specific depth (Mazen et al., 2021). It is the only technical method for establishing communication channels between surface operations and underground resources. Drilling technology plays a crucial role not only in the exploration and development of oil and gas but also in geothermal resource utilization, carbon dioxide storage, nuclear waste disposal, and other fields. Its significance lies in enabling the efficient development and utilization of underground resources.

Despite continuous technological advancements, the high cost of drilling operations remains a major bottleneck for the large-scale and economically viable development of deep underground resources. This challenge is particularly pronounced in deep and

* Corresponding author.
E-mail address: songxz@cup.edu.cn (X.-Z. Song).
Peer review under the responsibility of China University of Petroleum (Beijing).

https://doi.org/10.1016/j.petsci.2026.06.024
1995-8226/© 2026 Publishing services by Elsevier B.V. on behalf of KeAi Communications Co. Ltd. This is an open access article under the CC BY-NC-ND license (http://creativecommons.org/licenses/by-nc-nd/4.0/).

ultra-deep formations, where drilling operations are confronted with highly heterogeneous lithologies, low rock drillability, and extreme downhole conditions such as high temperature and high pressure (Soares et al., 2020). These factors often lead to increased mechanical wear, frequent drilling incidents, and prolonged non-productive time, thereby significantly reducing operational efficiency.

To address these challenges, drilling optimization technologies have been widely adopted to enhance drilling efficiency by minimizing non-drilling time, shortening the drilling cycle, and reducing overall costs (Ren et al., 2023). Among various performance indicators, the rate of penetration (ROP) is recognized as one of the most critical metrics for evaluating drilling efficiency. Accurate ROP prediction not only provides quantitative guidance for real-time drilling parameter adjustment but also serves as a foundation for drilling optimization and intelligent decision-making, ultimately contributing to improved drilling efficiency and cost-effectiveness (Zhou et al., 2022).

In recent years, the rapid advancement of artificial intelligence, information technology, data storage, and high-performance computing has sparked the “Fourth Industrial Revolution”. In the oil drilling sector, global oil and gas companies, along with research institutions, have recognized the immense potential of artificial intelligence and have made intelligent drilling a strategic research priority. Currently, scholars are exploring the application of artificial intelligence technology across various drilling scenarios and have achieved promising research outcomes (Li et al., 2022; Mahmoodzadeh et al., 2022). In the area of intelligent ROP prediction, many researchers have developed predictive models using various machine learning algorithms (Alsaihati et al., 2022; Gan et al., 2022; Höhn et al., 2022). These models utilize parameters from geological logging, mud logging, logging while drilling, and engineering logging data as inputs, with the ROP as the output parameter (Elmgerbi et al., 2021). Based on drilling data from a gas well in southern Iran, Zhao et al. (2020) constructed a ROP prediction model using an artificial neural network model. Safarov et al. (2022) established multiple ROP prediction models using linear regression, nonlinear regression, deep neural networks, random forests, and long short-term memory networks, and validated them in three different wells in the South Caspian Basin. The study found that the random forest model was the optimal model with an R^2 of 0.9. Yuan et al. (2025) proposed a real-time prediction method for ROP sequence based on bidirectional long short-term memory neural network. Based on the test results of field data, the average relative error of the established model is 3.53%. Gan et al. (2022) introduced the sliding window strategy and built a dynamic prediction method for ROP based on the extreme learning machine algorithm.

Some scholars use Bingham model, Hareland’s model, and machine learning algorithms to establish a ROP prediction model respectively, and compare the performance of traditional ROP equation and machine learning model through real drilling data (Hegde et al., 2017). Compared to traditional ROP prediction methods based on ROP equations and numerical simulations, intelligent ROP prediction models can effectively capture the complex relationships between multiple drilling parameters and ROP without relying on idealized assumptions (Gan et al., 2022). This capability enables more accurate and real-time ROP predictions, particularly in challenging deep-depth drilling environments. The intelligent ROP prediction method demonstrates significant advantages and holds great potential for further development (Barbosa et al., 2019).

However, as intelligent drilling technology continues to evolve, numerous intelligent ROP prediction models have been tested and applied in real drilling operations (Alsaihati et al., 2022; Gupta and Bhui, 2025; Zhou et al., 2023). Yet, data-driven ROP prediction models often struggle to fully meet the practical demands of real-world drilling environments (Feng et al., 2023; Jalakani and Tabatabaee Moradi, 2024; Li et al., 2022). In particular, the most widely used intelligent ROP prediction models are often not trusted by field experts due to their lack of interpretability and reliability in complex drilling conditions (Zhang et al., 2023; Zhao et al., 2020).

The primary reason for this lack of trust is the black-box nature of machine learning models. Intelligent ROP prediction models often suffer from unexplainable calculation processes, and in some cases, their predictions contradict fundamental physical laws (Pei et al., 2024a; Ren et al., 2023). These issues undermine the confidence of field experts in intelligent ROP predictions. Addressing these challenges is crucial, as they represent core obstacles to the advancement of intelligent drilling technology. Especially in deep drilling projects, which involve significant capital investment, numerous engineering personnel, and high operational risks, unreliable intelligent ROP predictions can mislead decision-making, potentially endangering both lives and property (Ma et al., 2024; Pei et al., 2024b). Therefore, a critical challenge in intelligent ROP prediction research is integrating drilling expertise with artificial intelligence algorithms to ensure that predictions align with objective physical laws (Pei et al., 2023). Overcoming this challenge is essential for improving the reliability and trustworthiness of intelligent ROP prediction models (Shimodaira, 2000; Yang et al., 2025; Zadrozny, 2004).

However, the application of intelligent ROP prediction in real drilling scenarios faces several challenges. First, actual drilling data is often sparse, locally concentrated, and highly discrete. Second, not all observed data points are reliable or suitable for reference due to issues such as noise or measurement errors. Third, there is often a significant difference in data distribution between the training set and the test set, which limits the generalization ability of the model and affects its performance in real-world applications. In 2019, Raissi et al. (2019) first introduced the physics-informed neural network (PINN), which enhances the solution process by embedding control equations derived from theoretical analysis directly into the learning framework. PINN incorporates initial conditions, boundary conditions, and governing physical equations into the total loss function, guiding the model to produce outputs that are more consistent with physical laws. This approach not only improves the physical interpretability of the predictions but also significantly reduces reliance on large training datasets, achieving strong performance even with limited data.

The proposal of PINN has provided a valuable source of inspiration and a foundational paradigm for integrating physical mechanisms with artificial intelligence. In response, many researchers have begun to explore, refine, and innovate intelligent modeling approaches that effectively combine physical principles with data-driven methods. Among these approaches, the most representative are broadly categorized into soft constraint models and hard constraint models, each offering distinct strategies for embedding physical knowledge into machine learning models (Chen et al., 2021).

The soft constraint method, primarily represented by PINN, operates by incorporating the governing equations of the physical model as regularization terms within the overall loss function (Jagtap et al., 2020; Yang and Perdikaris, 2019; Zhang et al., 2019). The objective of optimization is to minimize this total loss, which combines data fitting errors with physical information errors. To achieve this, the model’s weight and bias parameters are updated using gradient descent or other optimization algorithms. However, in practice, the prediction results of soft-constrained intelligent models may still be physically unreasonable or violate governing

equations in specific cases. This is because the soft constraint approach only enforces physical consistency in an average sense across the domain. It does not guarantee that the prediction results at every individual point strictly satisfies the physical constraints, which can be a significant limitation in safety-critical or high-precision deep drilling applications (Beucler et al., 2021; Yang et al., 2021).

In contrast to soft constraints, hard constraint machine learning methods strictly enforce the satisfaction of governing equations or predefined constraints during both the training and prediction phases of the model. These methods ensure that the machine learning outputs remain within the feasible solution space defined by physical or domain-specific requirements at all times (Xu and Darve, 2022). Two common hard constraint techniques are the projected gradient method and the Lagrange multiplier method: The projected gradient method works by projecting the results back onto the feasible domain after each gradient descent step. This approach is particularly effective for convex constraint problems, as it ensures the updated solution remains within the allowable region defined by the constraints (Mohan et al., 2020). The Lagrange multiplier method transforms the constrained optimization problem into an unconstrained one by introducing Lagrange multipliers. This method is more flexible, capable of handling both convex and non-convex problems, and directly incorporates constraint satisfaction into the optimization process. Hard constraint methods offer precise control over local solution spaces, allowing machine learning models to strictly adhere to physical laws or business rules where necessary. This is especially valuable in high-risk and high-investment fields such as deep drilling, where the accuracy and reliability of predictions are critical to operational safety and cost efficiency (Sheng and Yang, 2021).

In the field of ROP prediction, some scholars have begun to conduct intelligent modeling research under the constraints of physical mechanisms. Huang et al. (2024) incorporated drilling mechanical knowledge as a constraint into the loss function of ROP prediction model. Compared with the traditional intelligent model, the prediction accuracy of the knowledge constraint model for the target well was improved by 64.51%. Jiao et al. (2024) considered three methods, namely residual modeling, integrated coupling and simple averaging, and constructed an intelligent ROP prediction model combining mechanism and data. However, overall, the development of intelligent ROP prediction methods under physical constraints remains in its early stages and lacks a clear, standardized framework. Many existing approaches are still exploratory, and challenges such as model generalization, constraint enforcement, and real-time applicability persist. As a result, further research is needed to deepen theoretical foundation, improve methodological robustness, and promote practical implementation in complex and high-risk drilling environments.

In this study, a drilling knowledge constrained deep neural network (DCDNN) model is innovatively proposed for ROP prediction and drilling parameter optimization. The model integrates both soft constraints and hard constraints to embed domain-specific knowledge into the prediction process. Specifically, based on established ROP equations and engineering experience, the influence of weight on bit (WOB) and revolutions per minute (RPM) on the ROP, as well as their boundary conditions, are identified. Physical correlation knowledge is incorporated into the loss function via soft constraints, while boundary conditions are embedded directly into the output layer using hard constraints. This enables a seamless fusion of mechanistic knowledge with deep learning. With WOB and RPM set as control variables, and with the objectives of maximizing the ROP and minimizing the drill bit mechanical specific energy (BMSE), a dynamic optimization of control parameters during the drilling process is performed. The proposed model is validated using field data from seven ultra-deep wells in the Tarim Oilfield, China. Results show that the DCDNN ROP prediction model achieves a prediction accuracy of 81.91%, and post-optimization, the ROP improves by 51.09%. This study addresses the limitations of traditional data-driven models that often violate physical principles, significantly enhances the interpretability and reliability of intelligent drilling systems, and promotes the integration of artificial intelligence into deep underground resource development.

The main contributions of this study are as follows: 1) A systematic method is proposed for transforming complex drilling knowledge into a form that can be embedded into neural networks; 2) An intelligent ROP prediction model that integrates prior engineering knowledge is constructed; 3) A dynamic optimization method for drilling parameters based on ROP prediction is developed; 4) The effectiveness of the drilling knowledge constraint mechanism within the model is verified through interpretability analysis.

The organization structure of this paper is as follows: Section 2 introduces the relevant knowledge in the field of drilling and the principle basis of soft and hard constraints, proposes the DCDNN ROP prediction model, and constructs the overall workflow for dynamic optimization of drilling parameters; Section 3 constructs the DCDNN model based on real drilling data from the Tarim Oilfield, and conducts drilling parameter optimization experiments on the target wells; Section 4 conducts a detailed analysis and verification of the prediction accuracy and constraint reliability of the DCDNN ROP prediction model; Section 5 summarizes the main contents of this study.

2. Methodology

PINNs typically incorporate governing equations into neural networks through physics residuals. However, in deep drilling engineering, explicit and closed form governing equations for the ROP are rarely available, and domain knowledge is mainly expressed as empirical relationships, operational limits, and monotonic trends derived from field practice. These characteristics limit the direct applicability of conventional PINN frameworks.

To address this gap, this study proposes a drilling knowledge constrained deep neural network (DCDNN) that advances beyond traditional PINNs by embedding drilling knowledge as structured regularization mechanisms rather than equation-based residuals. Specifically, drilling knowledge expressed in Eqs. (1–3) is transformed into two complementary forms of constraints: (i) soft constraints, implemented as penalty terms in the loss function (Eqs. (13–15)) to guide learning toward physically consistent trends, and (ii) hard constraints, enforced through output-layer structures (Eqs. (19), (21) and (23)) to strictly satisfy operational boundaries.

The overall workflow consists of data preprocessing, drilling knowledge extraction, constraint embedding, constrained model training, performance validation, and drilling parameter optimization, as illustrated in Fig. 1. Using field data from seven ultra-deep wells, the DCDNN model demonstrates improved prediction accuracy, robustness, and physical plausibility compared with a purely data-driven DNN. Based on physically consistent predictions, a multi-objective optimization framework is further developed to maximize ROP while minimizing BMSE. By shifting physics-informed learning from equation-driven constraints to knowledge-driven regularization, the proposed DCDNN

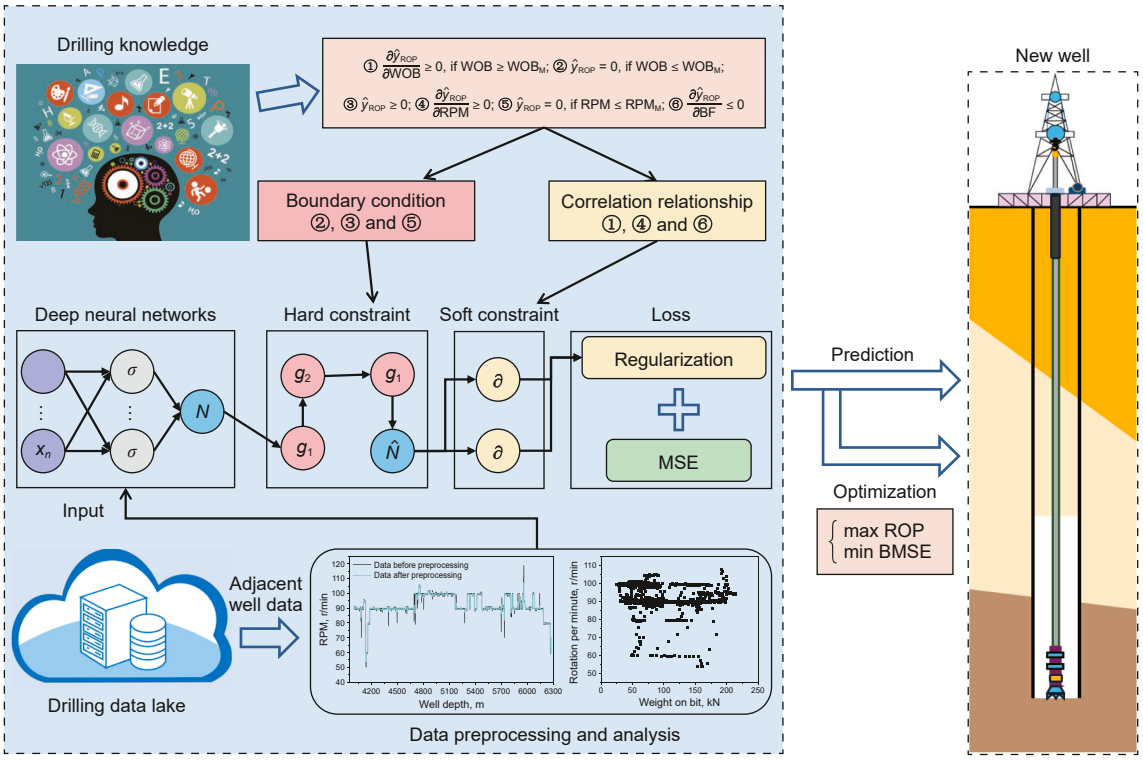


Fig. 1. Schematic diagram of the drilling optimization framework.

framework provides a practical and scalable solution for intelligent drilling optimization in complex subsurface environments.

2.1. Drilling knowledge

Once the drilling equipment used in an operation is determined, the ROP is primarily influenced by several key parameters, including bit wear, bottom-hole pressure differential, bottom-hole cleanliness, WOB, and RPM. To better understand the impact of these factors on ROP, scholars have conducted extensive research. Their findings have been expressed through various forms, including partial differential equations and explicit empirical equations, providing a theoretical basis for ROP prediction.

2.1.1. The performance constraint condition

Scholars have been studying the ROP for nearly 80 years, leading to the development of a series of ROP equations based on empirical and theoretical research (Maurer, 1962; Soares et al., 2020; Young, 1969). Among these, the modified Young's ROP equation is considered the most comprehensive and widely used. According to the modified Young's ROP equation, the ROP, along with influencing factors such as WOB, RPM, and bit wear, must satisfy specific physical and operational constraints. These relationships are mathematically represented by Eqs. (1–3).

$$\mathrm{ROP} \propto (\mathrm{WOB} - \mathrm{WOB_M}) \tag{1}$$

$$\mathrm{ROP} \propto \mathrm{RPM}^{\lambda} \tag{2}$$

$$\mathrm{ROP} \propto \frac{1}{1 + C_2 h} \tag{3}$$

where $\mathrm{WOB_M}$ is the threshold WOB, λ is the RPM index, h is the drill bit wear, C_2 is the drill bit wear coefficient.

In the actual drilling process, due to the lack of real-time monitoring methods, it is difficult to directly obtain the amount of drill bit wear. The drill bit footage (BF) refers to the total footage of the drill bit breaking the formation since it entered the well, in meters. According to the Archard wear theory model, under the assumption of constant WOB, the drill bit wear can be regarded as an approximate linear indicator of its cumulative BF (Waughman et al., 2002). Therefore, BF is employed in this study as a practical proxy for bit wear. However, it should be noted that BF represents a linear cumulative measure, whereas actual bit wear evolves through complex and nonlinear mechanisms influenced by lithology, loading conditions, and drilling dynamics. As a result, BF may not fully capture localized or abrupt wear variations, particularly in formation transition intervals. Future studies may further improve wear representation by incorporating formation-dependent wear indices or real-time downhole measurements.

2.1.2. The boundary constraint condition

The boundary conditions of mechanical drilling rate prediction refer to the various limiting factors and influencing conditions that must be accounted for during the rock-breaking process. These include constraints imposed by the geological environment, engineering equipment capabilities, and operational parameters. By incorporating boundary constraints from real drilling projects, the intelligent ROP prediction model can be aligned more closely with actual field conditions. This not only enhances the realism and reliability of predictions but also prevents unnecessary complexity caused by the unrestricted variation of input variables, thereby improving both the accuracy and practicality of the model's

outcomes. This study primarily considers three key boundary conditions in the intelligent ROP prediction: threshold WOB, threshold RPM, and the confidence interval of ROP.

The WOB threshold and RPM threshold represent the minimum WOB and RPM, respectively, required for the drill bit to penetrate the formation and initiate effective rock breaking. These threshold values can typically be estimated from logging data. When both the actual WOB and RPM exceed their respective thresholds, the bit teeth begin to engage the rock under the combined effects of axial force and torque, resulting in a ROP greater than zero. Conversely, if either parameter falls below its threshold, the drill bit cannot effectively fracture the formation, and the ROP remains zero. This physical process is formally represented by Eqs. (4) and (5).

$$\mathrm{ROP} = 0, \text{ if } \mathrm{WOB} \leq \mathrm{WOB_M}, \tag{4}$$

$$\mathrm{ROP} = 0, \text{ if } \mathrm{RPM} \leq \mathrm{PRM_M} \tag{5}$$

In addition, during actual drilling operations, the ROP cannot be negative. Therefore, the predicted ROP must also comply with the physical reality of being greater than or equal to zero, as specified in Eq. (6).

$$\mathrm{ROP} \geq 0 \tag{6}$$

2.2. Deep neural network

The ROP is influenced by a wide range of factors, including formation rock properties, engineering parameters, and drilling conditions. To date, there is no single predictive equation that comprehensively accounts for all these variables due to the complexity and nonlinear nature of their interactions. However, deep neural network (DNN) offers a promising solution. Renowned for their powerful nonlinear fitting capabilities, DNNs can effectively capture intricate patterns and relationships hidden within drilling data. By leveraging large volumes of multi-source input data, such as logging, mud logging, and surface parameters, deep neural networks can uncover latent features and correlations, enabling highly accurate predictions of ROP, even in complex and dynamic drilling environments.

As shown in Fig. 2(a), a DNN is composed of three fundamental components: the input layer, the hidden layers, and the output layer. The number of neurons in the input layer corresponds directly to the number of input features. Similarly, the number of neurons in the output layer matches the number of output features, which is typically one in the case of ROP prediction. Each hidden layer contains a varying number of neurons, depending on the model design. These neurons are responsible for processing the input data through two main steps: linear combination and activation function. Except for the input layer, the input to each neuron in the DNN is the output from the previous layer. While hidden layers typically apply an activation function (such as ReLU, tanh, or sigmoid), the output layer usually omits the activation function, especially in regression problems like ROP prediction, to allow for continuous-valued outputs. Through backpropagation and optimization algorithms, the DNN learns to minimize prediction loss, enabling accurate modeling of the complex dynamics involved in drilling operations.

For conventional regression models, prediction loss is commonly measured using the mean squared error (MSE), which

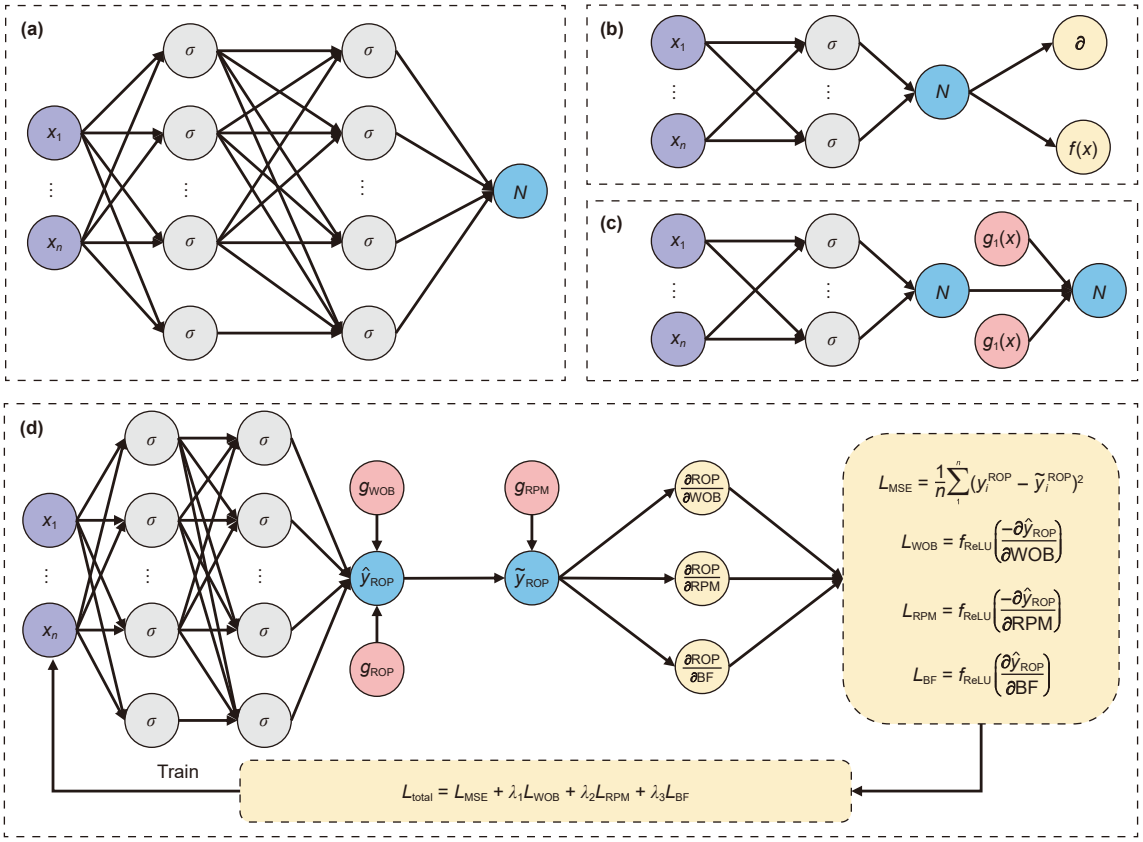


Fig. 2. Model structure of neural network: (**a**) DNN model; (**b**) soft constraint model; (**c**) hard constraint model; (**d**) DCDNN ROP prediction model.

quantifies the average squared difference between the predicted values and the actual observed values.

$$\mathrm{MSE} = \frac{1}{n}\sum_{1}^{n}(y_i - \widehat{y}_i)^2 \tag{7}$$

where n is the number of samples, y_i is the actual ith value of the sample, $\widehat{y}_i$ is the ith predicted value of the sample.

2.3. Physical constraints for neural networks

The current physical constraint methods applied to neural network models can be broadly categorized into two main types: soft constraints and hard constraints. Both approaches seek to enhance the interpretability, reliability, and versatility of neural network models by grounding them in established physical principles. However, their implementation mechanisms within neural networks differ significantly.

2.3.1. Soft constraint model

In a conventional regression neural network model, the loss function typically consists only of a MSE term. Soft constraints incorporate physical knowledge into neural networks by adding physical laws as penalty terms in the loss function, as shown in Fig. 2(b). The extent to which the model's predictions conform to known physical equations or empirical laws is measured through the penalty term loss. This approach offers a paradigm for enabling neural networks to learn from data under the guidance of physical principles, enhancing the model's learning capability while reducing the likelihood of non-physical or unreasonable predictions, particularly in cases with limited data or high levels of noise. However, soft constraints can only ensure that the model's predictions are approximately consistent with physical laws on average, and cannot guarantee strict compliance at every prediction point. Consequently, the model's output may still be unrealistic or clearly violate known physical mechanisms or governing equations.

The general form of the soft-constrained loss function can be expressed as:

$$L_{\mathrm{total}} = L_{\mathrm{MSE}} + \lambda L_{\mathrm{soft}} \tag{8}$$

where L_{total} is the total loss, L_{MSE} is the MSE loss, L_{soft} quantifies the model's violation of physical laws, λ is a weight coefficient that balances the influence of the soft physical constraint.

2.3.2. Hard constraint model

Hard constraints are implemented by explicitly embedding physical constraints into the architecture or computational process of a neural network, as shown in Fig. 2(c). In contrast to soft constraints, which incorporate physical laws as penalty terms in the loss function, hard constraints ensure that the governing equations are strictly satisfied within specific regions during both the training and prediction phases.

This is commonly achieved through techniques such as the projected gradient method, and the Lagrange multiplier method. The Lagrange multiplier method is primarily employed to handle equality constraints in optimization problems. By introducing Lagrange multipliers into the objective function, this method reformulates the original constrained optimization problem as an unconstrained one.

When there are equality boundary constraints as shown in Eq. (9) (Lu et al., 2021):

$$u(x) = g(x),\ x \in \Gamma_{\mathrm{D}} \tag{9}$$

In order for the output of the DNN model to meet this boundary condition, construct the function shown in Eq. (10):

$$u(x) = g(x) + \ell(x)N(x,w),\ x \in \Omega \tag{10}$$

where is Γ_{D} the subdomain of the boundary condition, Ω is the domain of x, $u(x)$ is the feasible domain of the target value, $g(x)$ is the value on the boundary, $N(x,w)$ is the output of the neural network, $\ell(x)$ is the distance function, and satisfies the following conditions:

$$\begin{cases} \ell(x) = 0,\ x \in \Gamma_{\mathrm{D}} \\ \ell(x) > 0,\ x \in \Omega - \Gamma_{\mathrm{D}} \end{cases} \tag{11}$$

2.4. ROP intelligent prediction constrained by drilling knowledge

2.4.1. Drilling knowledge extraction

Based on the drilling physics principles summarized in Section 2.1, the optimization of the ROP prediction model is formulated as a multi-condition constrained optimization problem, as shown in Eq. (12). There are three performance constraints: WOB, RPM, and BF; three boundary constraints: WOB threshold, RPM threshold, and ROP confidence interval.

$$\begin{aligned} &\min_{w,b} \sum (y_{\mathrm{ROP}} - \widehat{y}_{\mathrm{ROP}})^2 \\ &\text{s.t.} \quad \frac{\partial \widehat{y}_{\mathrm{ROP}}}{\partial \mathrm{WOB}} \geq 0,\ \text{if WOB} \geq \mathrm{WOB_M}, \\ &\widehat{y}_{\mathrm{ROP}} = 0,\ \text{if WOB} \leq \mathrm{WOB_M}, \\ &\frac{\partial \widehat{y}_{\mathrm{ROP}}}{\partial \mathrm{RPM}} \geq 0, \\ &\widehat{y}_{\mathrm{ROP}} = 0,\ \text{if RPM} \leq \mathrm{RPM_M}, \\ &\frac{\partial \widehat{y}_{\mathrm{ROP}}}{\partial \mathrm{BF}} \leq 0, \\ &\widehat{y}_{\mathrm{ROP}} \geq 0, \end{aligned} \tag{12}$$

where y_{ROP} is the measured value of ROP, $\widehat{y}_{\mathrm{ROP}}$ is the neural networks predicted value of ROP.

2.4.2. Drilling knowledge transformation

The constraints expressed in Eq. (12) are difficult to incorporate directly into the neural network's computation and optimization process. Therefore, they must be transformed into a form compatible with neural network training, typically using soft constraints or hard constraints.

For the performance constraints defined in Eq. (12), this study adopts a soft constraint strategy by integrating them as penalty terms in the neural network's loss function. Specifically, the constraints are transformed using a barrier function, which adds a penalty only when the constraint is violated. A key characteristic of the chosen barrier function is that: the penalty remains zero when the constraint is satisfied, and the penalty increases rapidly when the constraint is violated. To achieve this behavior, this study employs the ReLU function as the barrier function. The performance constraints on WOB, RPM, and BF presented in Eq. (12) can be reformulated into the forms shown in Eqs. (13–15), respectively.

$$L_{\mathrm{WOB}} = f_{\mathrm{ReLU}}\left(\frac{-\partial \hat{y}_{\mathrm{ROP}}}{\partial \mathrm{WOB}}\right) \tag{13}$$

$$L_{\mathrm{RPM}} = f_{\mathrm{ReLU}}\left(\frac{-\partial \hat{y}_{\mathrm{ROP}}}{\partial \mathrm{RPM}}\right) \tag{14}$$

$$L_{\mathrm{BF}} = f_{\mathrm{ReLU}}\left(\frac{\partial \hat{y}_{\mathrm{ROP}}}{\partial \mathrm{BF}}\right) \tag{15}$$

Given that the positive correlation between WOB and ROP is already introduced as a soft constraint term in Eq. (13), the WOB threshold hard constraint (originally described in Eq. (4)) can be simplified. The revised strategy proposed in this study enforces that when the WOB equals the threshold value, the predicted ROP output by the neural network is forced to be zero, as shown in Eq. (17). This approach preserves the physical interpretation of the threshold WOB condition, no rock-breaking action occurs below the threshold WOB, while avoiding training instability. Accordingly, the original form of the hard constraint in Eq. (12) is structurally optimized and reformulated, with the improved expression shown in Eq. (17), and the hard constraint formulation for the WOB threshold is presented in Eqs. (18) and (19).

$$\mathscr{C}_{\mathrm{WOB}} = f_{\mathrm{ReLU}}(\mathrm{WOB} - \mathrm{WOB_M}) \tag{16}$$

$$\begin{cases} \mathrm{ROP} = 0, \ \text{when } \mathrm{WOB} = \mathrm{WOB_M} \\ \mathrm{ROP} \propto (\mathrm{WOB} - \mathrm{WOB_M}) \end{cases} \tag{17}$$

$$\mathscr{C}'_{\mathrm{WOB}} = \mathrm{WOB} - \mathrm{WOB_M} \tag{18}$$

$$g_{\mathrm{WOB}}(\mathrm{WOB}, \hat{y}_{\mathrm{ROP}}) = 0 + \mathscr{C}'_{\mathrm{WOB}}\hat{y}_{\mathrm{ROP}} \tag{19}$$

Similarly, the hard constraint formulations for the RPM threshold are presented in Eqs. (20) and (21).

$$\mathscr{C}_{\mathrm{RPM}} = \mathrm{RPM} - \mathrm{RPM_M} \tag{20}$$

$$g_{\mathrm{RPM}}(\mathrm{RPM}, \hat{y}_{\mathrm{ROP}}) = 0 + \mathscr{C}_{\mathrm{RPM}}\hat{y}_{\mathrm{ROP}} \tag{21}$$

For the confidence interval of ROP, a distance function is constructed using the ReLU functions, as shown in Eq. (22). The hard constraint formulation for the confidence interval of ROP is presented in Eq. (23).

$$\mathscr{C}_{\mathrm{ROP}} = f_{\mathrm{ReLU}}(\hat{y}_{\mathrm{ROP}}) \tag{22}$$

$$g_{\mathrm{ROP}}(\hat{y}_{\mathrm{ROP}}) = 0 + \mathscr{C}_{\mathrm{ROP}}\hat{y}_{\mathrm{ROP}} \tag{23}$$

2.4.3. Drilling knowledge constrained DNN model

To effectively embed drilling knowledge into the DNN computation process, this study proposes a drilling knowledge constrained deep neural network (DCDNN) model, as shown in Fig. 2(d). This intelligent prediction model integrates both hard constraints and soft constraints to enhance the physical interpretability and reliability of the ROP predictions. Built upon the standard DNN architecture, the DCDNN model incorporates engineering expertise and physical laws from the drilling domain, enabling a hybrid modeling approach that combines data-driven learning with mechanism-based understanding.

The input and hidden layer structures of the DCDNN model are consistent with those of a traditional DNN, primarily responsible for the nonlinear extraction and combination of input features. However, the output layer of the DCDNN model incorporates a hard constraint mechanism grounded in engineering knowledge. This mechanism explicitly enforces boundary condition constraints, including the WOB threshold, RPM threshold, and the ROP confidence interval, as formulated in Eqs. (19), (21) and (23), respectively. In contrast to standard DNNs, the DCDNN model introduces a hard constraint computation unit, described in Eq. (24), within the output layer to embed these constraints directly into the neural network's prediction process.

$$\tilde{y}_{\mathrm{ROP}} = g_{\mathrm{ROP}}(g_{\mathrm{RPM}}(\mathrm{RPM}, g_{\mathrm{WOB}}(\mathrm{WOB}, \hat{y}_{\mathrm{ROP}}))) \tag{24}$$

where $\tilde{y}_{\mathrm{ROP}}$ is the final prediction of ROP of DCDNN model.

In addition to the hard constraint mechanism embedded in the output layer, the DCDNN model also incorporates soft constraint penalty terms at the loss function level to further capture the physical correlations among key variables in the drilling domain. Specifically, based on established domain knowledge regarding the positive or negative correlations between the ROP and factors such as WOB, RPM, and BF, this study introduces three corresponding soft constraint terms into the loss function. These terms align with the correlation relationships defined in Eqs. (13–15). To regulate the influence of each soft constraint on model training, three tunable constraint weighting coefficients are introduced, λ_1, λ_2, and λ_3. These coefficients allow flexible control over the strength of each constraint's impact. The final loss function of the DCDNN model is defined as shown in Eqs. (25) and (26).

$$L_{\mathrm{MSE}} = \frac{1}{n}\sum_{1}^{n}\left(y_i^{\mathrm{ROP}} - \tilde{y}_i^{\mathrm{ROP}}\right)^2 \tag{25}$$

$$L_{\mathrm{total}} = L_{\mathrm{MSE}} + \lambda_1 L_{\mathrm{WOB}} + \lambda_2 L_{\mathrm{RPM}} + \lambda_3 L_{\mathrm{BF}} \tag{26}$$

2.5. Advanced drilling optimization based on intelligent ROP prediction

Based on the constructed DCDNN ROP prediction model, this study further explores drilling parameter optimization, with WOB and rotational speed selected as the primary control variables, aiming to enhance drilling efficiency and reduce operational costs.

2.5.1. Drilling optimization objective

In deep and complex formations, drilling operations are challenged by extreme downhole conditions such as high pressure and temperature, dense and hard rock formations, and increased mechanical resistance. Therefore, the optimization objectives in deep drilling go beyond simply increasing ROP. Instead, a more balanced approach is required: enhances overall energy efficiency while ensuring operational safety, equipment reliability, and cost-effectiveness. This overarching objective is further refined into two specific goals: maximizing ROP, and minimizing drilling bit mechanical specific energy (BMSE). BMSE refers to the mechanical energy required to crush a unit volume of rock. Lowering BMSE improves energy efficiency, reduces mechanical stress on the drilling system, and extends the service life of the drill bit. The formulation of BMSE is given by Eq. (27).

$$\mathrm{BMSE} = \frac{W_{\Delta t}}{V_{\Delta t}} = \frac{4\cdot \mathrm{WOB}}{\pi d_{\mathrm{b}}^2} + \frac{480\cdot \mathrm{RPM}\cdot \mathrm{Tor}}{d_{\mathrm{b}}^2\cdot \mathrm{ROP}} \tag{27}$$

where $W_{\Delta t}$ represents the energy required for rock crushing, $V_{\Delta t}$ represents the volume of rock crushed, Tor represents the torque, and d_{b} represents the diameter of the drill bit.

2.5.2. Drilling control parameters

In practical drilling operations, most parameters are predetermined or difficult to adjust dynamically due to constraints

imposed by equipment configuration, formation characteristics, and operational protocols at the well site. However, among these parameters, WOB and RPM are notable for their operational flexibility and significant influence on both the ROP and the BMSE. As such, this study identifies WOB and RPM as the primary control variables for drilling optimization. Nonetheless, it is important to recognize that adjustments to WOB and RPM are not without limits. Specifically, excessive WOB may cause severe drill bit wear or even lead to structural failure, and excessive RPM can induce undesirable downhole dynamics. To ensure that the optimization results are not only theoretically effective but also practically implementable, this study defines the operational control bounds of WOB and RPM according to industry standards and conventional drilling practices. These control bounds are expressed in Eq. (28).

$$\begin{cases} 0 \le \mathrm{WOB} \le 160 \\ 0 \le \mathrm{RPM} \le 100 \end{cases} \tag{28}$$

2.5.3. Multi-objective optimization of drilling parameters

In deep and complex drilling operations, multiple performance indicators often exhibit conflicting relationships. For example, increasing WOB generally enhances ROP. However, it may also lead to increased drill bit wear and increased BMSE, which in turn affects energy efficiency and operational safety. Therefore, optimizing drilling parameters based on a single objective is insufficient and may lead to suboptimal or even counterproductive results.

Accordingly, the optimization of drilling parameters is formalized as a multi-objective optimization problem, as described in Eq. (29):

$$\min_{x \in Z} [\, -f_{\mathrm{ROP}}(x), f_{\mathrm{BMSE}}(x)\,] \tag{29}$$

where x= [WOB, RPM], which is the drilling control parameter to be optimized; and Z is the optimization interval of WOB and RPM, as shown in Eq. (28).

To comprehensively balance the relationship between ROP and BMSE, the ratio of BMSE to ROP is often minimized as the objective function. This approach facilitates coordinated optimization of drilling efficiency and energy consumption, as shown in Eq. (30).

$$\min_{x \in \Lambda} \left[\frac{f_{\mathrm{BMSE}}(x)}{f_{\mathrm{ROP}}(x)} \right] \tag{30}$$

2.5.4. Drilling parameter optimization process

As shown in Fig. 3, the optimization of drilling parameters based on the intelligent ROP prediction involves the following three main steps:

Step 1: Drilling data preprocessing.

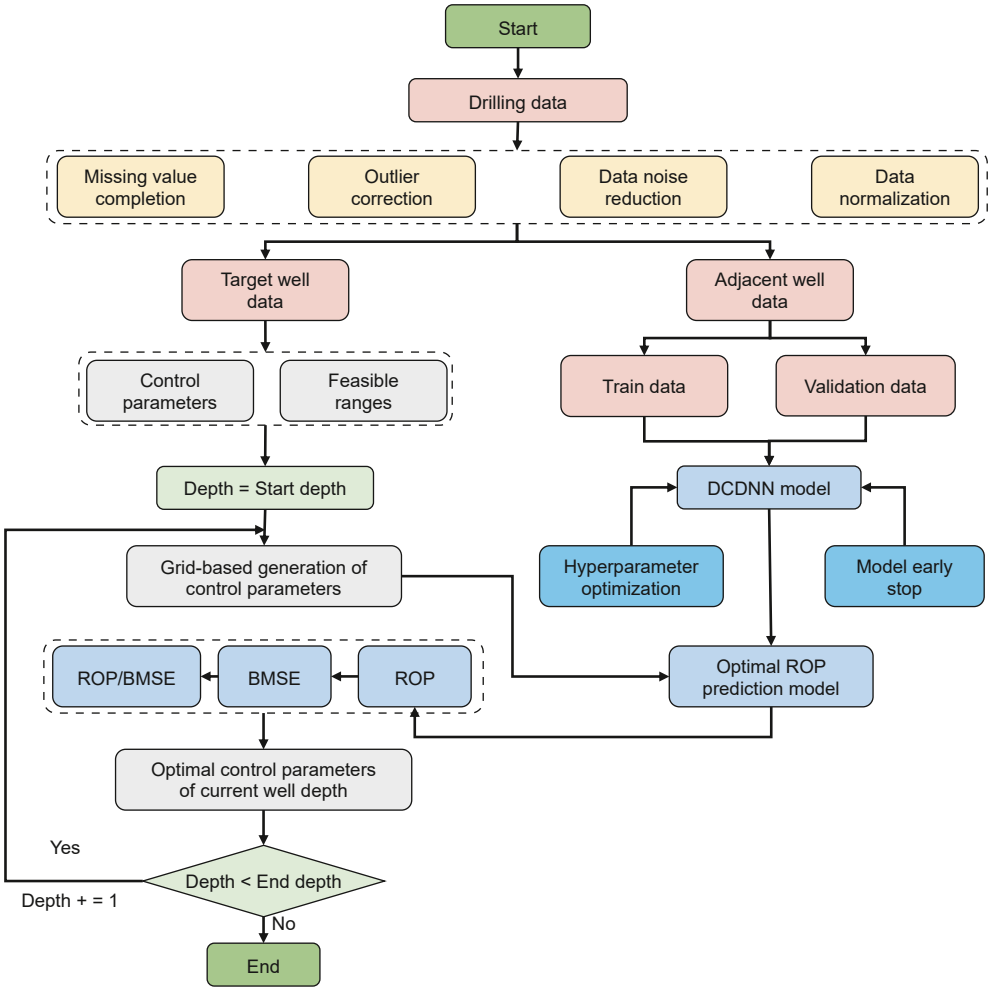


Fig. 3. Schematic diagram of drilling parameter optimization process.

Key drilling features are extracted from geological logging, engineering logging, and real-time drilling logs to serve as input variables for the model. To address issues such as missing values, outliers, and noise in the original data, a combination of data analysis techniques and domain-specific drilling knowledge is employed for data cleaning and normalization. One representative well is designated as the target well, while the remaining wells are randomly split into a training set (80%) and a validation set (20%).

Step 2: Construction of the DCDNN ROP prediction model.

The training set is used to train the DCDNN model, while the validation set is employed to monitor model performance and mitigate overfitting. Hyperparameter tuning is performed using optimization techniques such as Bayesian optimization to identify the optimal model configuration, thereby yielding a high-precision ROP prediction model.

Step 3: Drilling parameter optimization.

Taking the minimum depth of the target well as the starting point and the maximum depth as the endpoint, a depth-by-depth dynamic optimization process is conducted in the direction of increasing well depth. First, control variables (WOB and RPM) and their feasible operational ranges are determined. All possible combinations within the value ranges are generated using a grid search approach. For each parameter combination, the ROP is predicted using the trained DCDNN model, and the corresponding ROP and BMSE are computed. Taking the optimization objective function defined in the minimization equation (Eq. (30)) as the criterion, the optimal solution that satisfies "the optimized ROP is higher than the original ROP" is searched to obtain the optimal control parameters corresponding to the well depth. Repeat the above process to complete the dynamic optimization within the entire well section.

3. Experiment

3.1. Drilling data

3.1.1. Data background

The Tarim Basin, located in western China, is the largest superimposed composite basin in the country and one of the most important regions for oil and gas resources. However, the oil and gas deposits in this area are generally deeper than 6000 m. During the drilling process, it is necessary to cross multiple sets of strata with complex structures and variable lithologies. The operating environment is harsh, and the engineering difficulty is extremely high. Among them, the average burial depth of the Paleogene Kumugeliemu strata is about 5089 m, and the average layer thickness is about 2340 m, but its average ROP is only 9.57 m/h, which seriously restricts the drilling efficiency, resulting in extended cycles and increased costs, and has become an important bottleneck for the efficient development of deep oil and gas.

Table 1
Drilling characteristics input into the neural network.

Parameter type	Parameter name
Geological	Acoustic, gamma ray, lithology, formation pressure
Well deviation	Well inclination, well azimuth, wellbore curvature
Engineering	Well depth, vertical depth, revolutions per minute, torque, weight on bit, standpipe pressure, inlet flow rate, hook load
Drilling fluid	Mud density, mud viscosity, mud plastic viscosity
Drilling equipment	Bit footage, drill bit size

It is urgent to build a drilling parameter optimization technology system with dynamic response capabilities and high prediction accuracy. To this end, this study focuses on the deep Paleogene Kumugeliemu strata and conducts research on ROP prediction and drilling parameter optimization, aiming to integrate data-driven learning with drilling physical knowledge to support intelligent drilling optimization in deep and complex formations.

As shown in Fig. 4 and Table 1, The dataset used in this study is derived from the measured drilling data of 7 typical ultra-deep wells in the Tarim Oilfield area of China, covering multi-source information such as geological logging data, mud logging data, drilling equipment mechanical parameters and drilling logs during the entire drilling process. Among the seven selected wells, Well A11 is geographically located near the center of the study region and exhibits strong representativeness in terms of formation and drilling conditions. Therefore, it was selected as the target well to serve as the test set for evaluating the prediction accuracy of the model. The drilling data from the remaining six wells were used to construct the training and validation datasets. Fig. 5 illustrates the distribution of WOB and RPM for both the training set and the test set. As observed in the figure, the drilling parameter data exhibit a high degree of concentration within a specific range. This clustering indicates that most operational parameters are concentrated within a limited range, which motivates the incorporation of physical constraints to enhance model robustness in data-sparse regions. Nevertheless, the core distribution range of WOB and RPM in the test set closely aligns with that of the training set. This high degree of overlap enhances the model's adaptability and

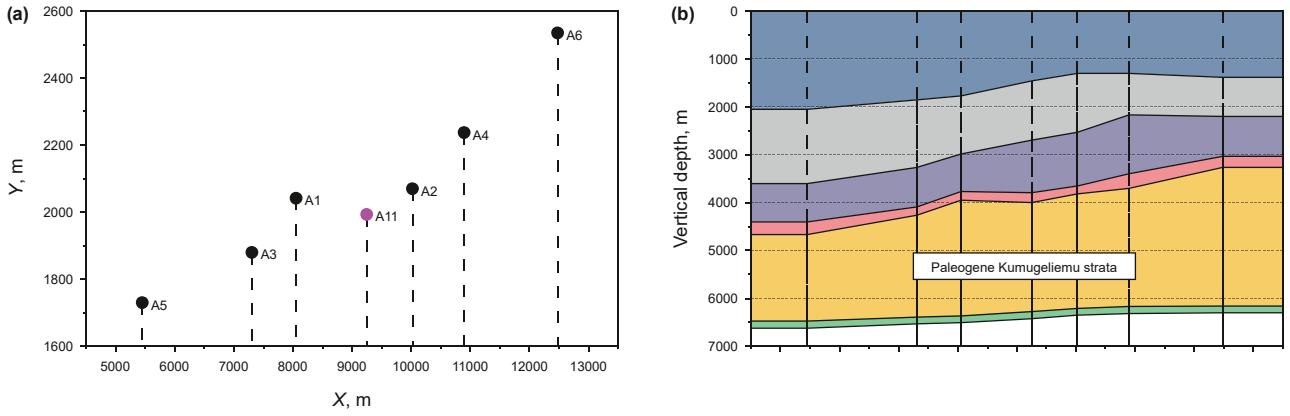


Fig. 4. Drilling data geological distribution map: (**a**) Well location distribution; (**b**) stratigraphic changes.

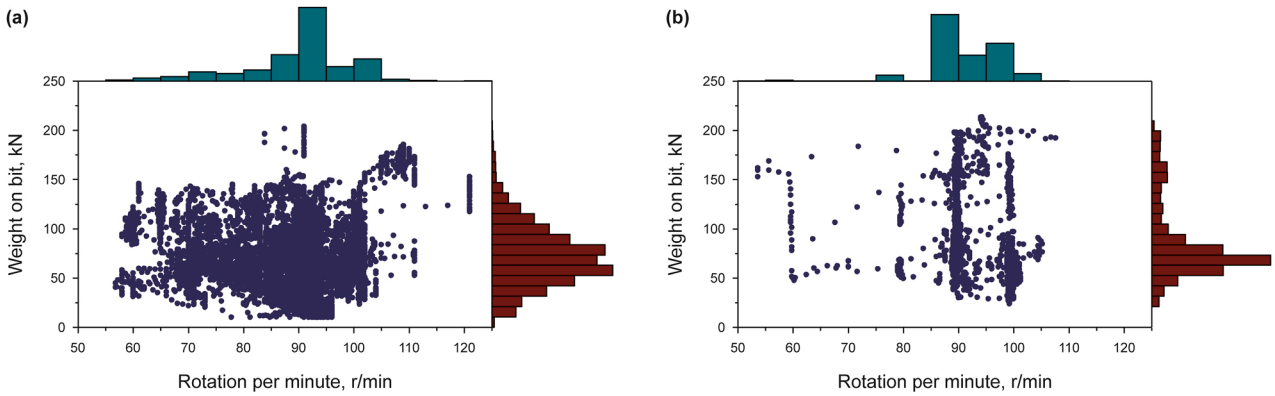


Fig. 5. Distribution diagram of WOB and RPM: (**a**) Other six wells; (**b**) Well A11.

reliability during the testing phase, effectively reducing prediction errors caused by distributional discrepancies between training and test data.

3.1.2. Data preprocessing

Due to differences in data acquisition equipment and operational environments, heterogeneity exists in the sampling intervals of various drilling data sources. For instance, the sampling interval of geological logging data is typically 0.3 m, while that of mud logging data is 1 m. To achieve effective fusion and alignment of multi-source data, this study uses the well depth from logging data as a unified reference and applies linear interpolation to synchronize data across different sources.

Based on an analysis of drilling conditions and a comprehensive feature selection process, a total of 16,381 valid samples were extracted. Each sample contains 20 feature variables, encompassing essential information such as formation characteristics, drilling parameters, and equipment operational status.

To ensure data integrity, the adjacent mean method is employed to impute abnormal and missing values, which may arise from equipment malfunctions or signal transmission losses. To further mitigate noise's impact on model performance, signal denoising was conducted by employing a Haar wavelet transform with a decomposition level of 2 and a 50% threshold applied at each level. As shown in Fig. 6, a comparison of the raw and preprocessed drilling data confirms that the adopted preprocessing strategy effectively enhances data quality and model robustness.

The statistical characteristics of selected drilling parameters are summarized in Table 2, including the mean, standard deviation, minimum, and maximum values for each feature. As an illustrative example, the average inlet density is 2.3, whereas the average well depth reaches 5090.4. The disparity between these two values

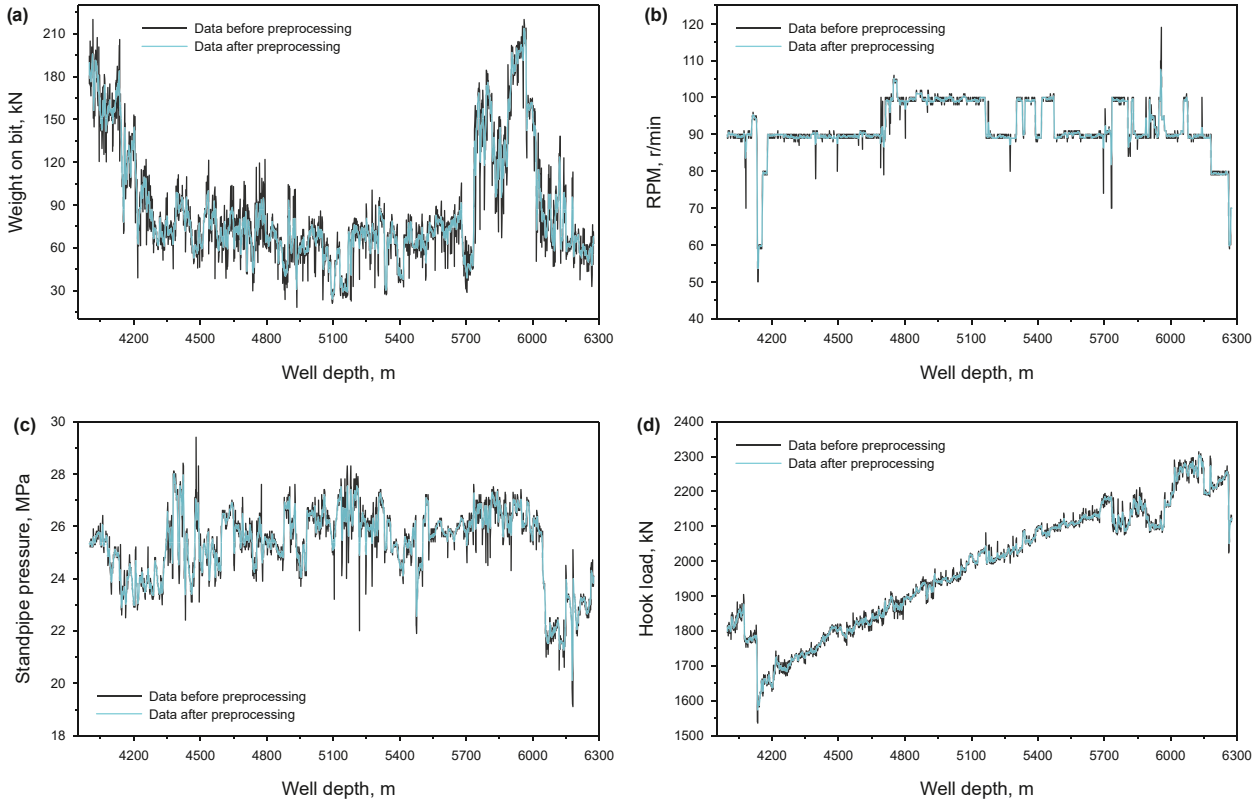


Fig. 6. Comparison of drilling data before and after preprocessing: (**a**) Weight on bit; (**b**) revolutions per minute; (**c**) standpipe pressure; (**d**) hook load.

Table 2
Statistics of some drilling characteristics.

Type	Depth, m	WOB, kN	RPM, r/min	SPP, MPa	Inlet flow rate, L/min	Mud density, g/cm^3	ROP, m/h
Mean	5090	75.0	89.9	23.9	1645.65	2.3	12.3
Standard deviation	738.5	32.3	9.1	2.1	482.1	0.2	8.7
Minimum	3262	10	53.6	7.3	565.6	1.7	0.5
Maximum	6475	213.8	121.0	28.5	3600.0	2.4	30.0

exceeds a factor of 2200, reflecting a significant difference in magnitude. Such disparities can lead to features with larger numeric scales disproportionately influencing the neural network's learning process during training. This imbalance not only hinders model convergence but may also degrade prediction accuracy. To mitigate this issue, all feature variables are standardized to a common scale, thereby eliminating differences in order of magnitude and ensuring that each feature contributes equally during model training. The standardization process adopted in this study is shown in Eq. (31).

$$x_i' = \frac{x_i - \mu_i}{\sigma_i} \tag{31}$$

where x_i is the value of the ith drilling feature, μ_i is the average value of the ith drilling features, σ_i is the standard deviation of the ith feature, and x_i' is the ith feature value after standardization.

3.2. ROP intelligent prediction based on DCDNN

Based on the DCDNN, Well A11 was designated as the target well for evaluating model prediction accuracy. The training dataset was constructed using 80% of the drilling data from six adjacent wells to train the intelligent ROP prediction model. During the training process, an early stopping mechanism was employed to monitor the model's validation error in real time, effectively mitigating the risk of overfitting. Specifically, training was automatically terminated when the validation loss failed to show significant improvement over several consecutive iterations. To further enhance model performance, this study conducted a hyperparameter optimization process targeting key configurations of the DCDNN ROP prediction model, including the learning rate, number of neurons in hidden layers, activation function types, and regularization coefficients. Bayesian optimization was adopted as the search algorithm due to its efficiency in navigating the hyperparameter search space, enabling rapid identification of optimal configurations. This significantly improved both model convergence speed and prediction accuracy. The final selected hyperparameter settings are presented in Table 3.

Fig. 7(a) presents a comparison between the measured ROP and the ROP predicted by the DCDNN model for the Paleogene Kumugeliemu strata of Well A11. As shown in the figure, the predicted ROP closely follows the overall trend of the measured ROP across most well intervals, demonstrating strong consistency. Notably, the model exhibits excellent fitting performance in the depth ranges of 4200–5000 and 5500–5900 m, which highlights the DCDNN model's robust capability in capturing the nonlinear relationships and complex patterns inherent in deep formation drilling data.

Fig. 7(b–e) present local enlarged views of the predicted and measured ROP for Well A11 at depths of 4200–4300, 4500–4600, 4700–4800, and 5700–5760 m, respectively. These detailed views further illustrate that the predicted ROP values generally fluctuate around the measured values and accurately capture the local variation trends. This confirms the DCDNN model's capacity to reflect detailed dynamic changes in key intervals of the well. It is noteworthy that prediction errors are relatively larger in segments where the measured ROP exhibits abrupt fluctuations, such as sudden increases or decreases. These anomalies often correspond to complex downhole conditions or sensor disturbances. Although the DCDNN model does not fully replicate all extreme ROP variations in these regions, it effectively captures the underlying trend while avoiding overfitting to outliers or noise. This trend-focused modeling strategy enhances the robustness and generalization ability of the model, ensuring reliable performance when applied to new well sections or under varying drilling conditions.

Fig. 7(f) presents a bar chart evaluating the prediction errors of the DCDNN model across the training set, validation set, and test set, comparing three key performance metrics: MSE, loss function value (Loss), and mean relative error (MRE). The results show that the model achieves MSE, Loss, and MRE values of 1.80, 1.85, and 9.71% on the training set, respectively; 2.37, 2.42, and 11.95% on the validation set; and 10.84, 10.85, and 15.92% on the test set. These results indicate that the model exhibits strong fitting capability on both the training and validation sets, with low errors and stable performance. Although the error metrics on the test set are higher than those on the training and validation sets, they remain within an acceptable range, demonstrating the model's generalization ability and robustness in practical prediction scenarios. Notably, the MRE difference between the training set and test set is only 6.21%, indicating that the model retains considerable accuracy when applied to previously unseen data. This performance further confirms the effectiveness of incorporating soft and hard constraint mechanisms in enhancing the generalization and reliability of the DCDNN model, offering solid support for intelligent ROP prediction and parameter optimization in complex drilling environments.

Table 3
Hyperparameters of the optimal DCDNN ROP prediction model.

Hyper-parameters	Evaluated range	Values
Input dimension	Determined by feature set	20
Output dimension	Fixed	1
Hidden layers	[4, 5, 6, 7]	6
Neurons (for each layer)	[64–256]	128, 128, 128, 96, 96, 96
Activation function	{ReLU, LeakyReLU, Tanh}	ReLU
Learning rate	[1e-4, 5e-4, 1e-3, 5e-3,1e-2]	0.001
Epoch	[2000–6000]	5000
Weight for L_{WOB}	[1e-5–0.5]	0.27
Weight for L_{RPM}	[1e-5–0.5]	0.12
Weight for L_{BF}	[1e-5–0.5]	0.01

3.3. Drilling parameter optimization

Taking the drilling parameter optimization at a well depth of 4953 m as an example, and holding all other parameters constant, the effects of WOB and RPM on the ROP and BMSE are illustrated in Fig. 8(a) and (b), respectively. Fig. 8(a) illustrates that in regions of low WOB and RPM (particularly when WOB and RPM approach zero), the ROP approaches zero, exhibiting clear boundary constraint characteristics. This aligns with the physical understanding that rock cannot be effectively broken without sufficient

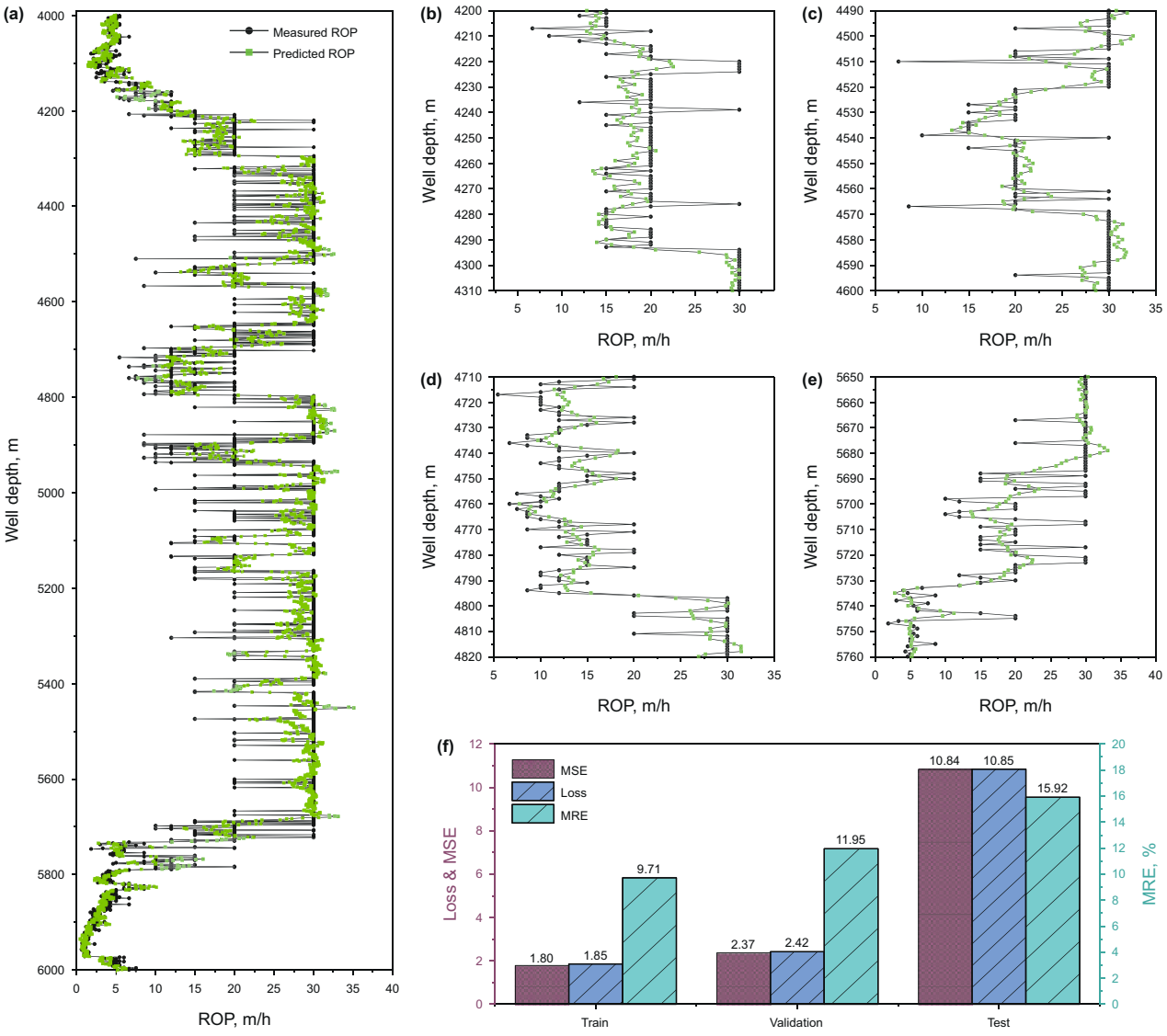


Fig. 7. Performance of DCDNN ROP prediction model: (**a**) Comparison of ROP predictions for Well A11; (**b**) comparison of ROP predictions from 4200 to 4310 m for Well A11; (**c**) comparison of ROP predictions from 4490 to 4600 m for Well A11; (**d**) comparison of ROP predictions from 4710 to 4820 m for Well A11; (**e**) comparison of ROP predictions from 5650 to 5760 m for Well A11; (**f**) performance on training, validation, and test sets.

force applied to the bit. As both WOB and RPM increase, the ROP increases substantially, exhibiting a nonlinear growth trend. This behavior indicates that the model effectively captures the coupled relationship between WOB, RPM, and ROP, and highlights the DCDNN model's ability to incorporate physical drilling knowledge through embedded soft constraints. Fig. 8(b) shows that in regions with low WOB and low RPM, the ROP is low while BMSE is high, resulting in significant energy inefficiency. As the control parameters increase, BMSE generally decreases, indicating improved drilling efficiency and reduced energy required per unit volume of rock. However, a slight rebound in BMSE is observed in certain regions of high WOB and high RPM, suggesting potential inefficiencies such as increased bit wear or energy wastage under extreme operational conditions. These results further validate the model's ability to capture realistic physical behaviors and guide practical drilling parameter optimization.

According to the control parameters and their operable ranges defined in Section 2, the feasible domain for WOB is [0, 160] kN, and for RPM is [0, 100] r/min. Within this domain, the two-dimensional distribution of ROP is shown in Fig. 9(a). As illustrated, the optimal combination of control parameters is in the lower-right region of the figure, where drilling efficiency is maximized, and energy consumption is minimized. The orange curve in the figure represents the Pareto frontier, reflecting the best trade-offs between ROP and BMSE. The point marked on the curve (ROP of 46.221 m/h and BMSE of 0.024 MPa) represents the optimal balance between drilling efficiency and energy utilization. Fig. 9(b) presents the three-dimensional distribution of the optimization objective function, defined as BMSE/ROP. It is evident that the minimum region of the objective function corresponds to a high WOB combined with a medium-to-high RPM. In contrast, the region characterized by low WOB and high RPM shows significantly higher values of BMSE/ROP, indicating low drilling efficiency and high energy consumption. Such parameter combinations are suboptimal and should be avoided in practice for efficient drilling operations.

To ensure that the optimized drilling parameters lead to a meaningful improvement in drilling efficiency, this study introduces a constraint condition: the optimized ROP must exceed the original ROP. The feasible solutions that satisfy this condition,

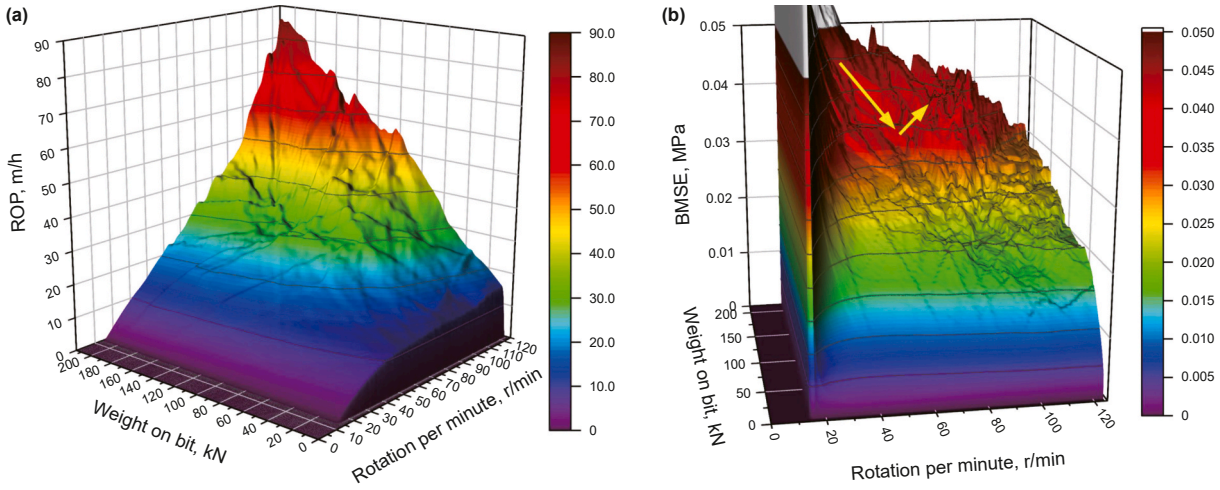


Fig. 8. 3D distribution diagram of the influence of control parameters on drilling: (**a**) ROP; (**b**) BMSE.

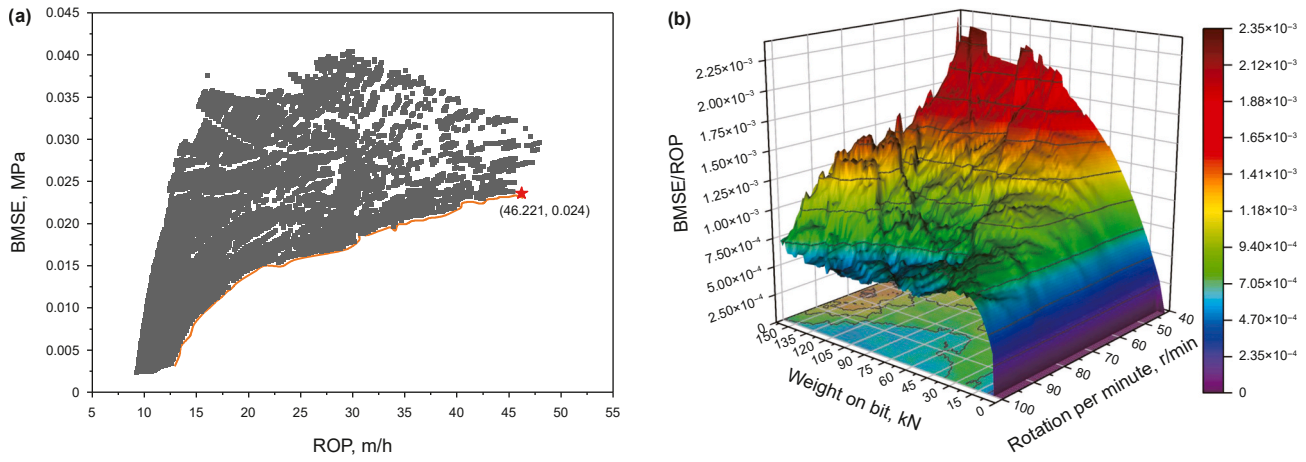


Fig. 9. Distribution of control parameters and optimization results: (**a**) Two-dimensional distribution of WOB and ROP within the feasible control parameter domain; (**b**) three-dimensional distribution of WOB, RPM, and BMSE/ROP across the feasible region.

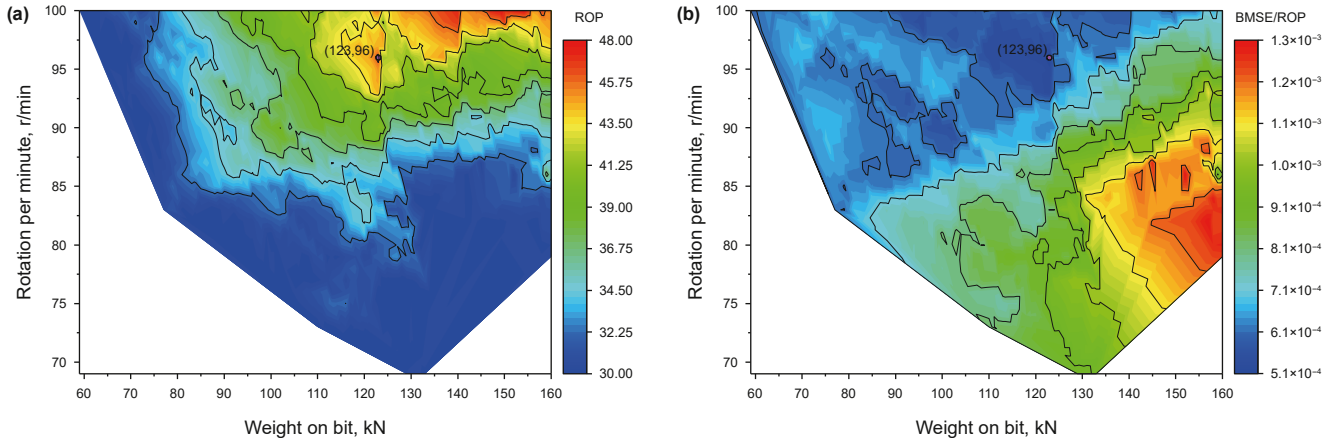


Fig. 10. Distribution of drilling performance indicators within the feasible control parameter domain: (**a**) ROP; (**b**) BMSE/ROP.

along with their corresponding WOB, RPM, ROP, and BMSE/ROP values, are illustrated in Fig. 10(a) and (b). As shown in Fig. 10, the optimal parameter combination occurs at WOB of 123 kN and RPM of 96 r/min, where the BMSE/ROP reaches its minimum value, indicating the most efficient balance between ROP and BMSE. The ROP corresponding to this optimal point is 46.22 m/h, and the BMSE is 0.02356 MPa. Compared with the pre-optimization parameters (WOB of 55.96 kN, RPM of 99.6 r/min, ROP of 30 m/h,

BMSE of 0.01698 MPa), the optimized scheme results in a ROP increase of 16.22 m/h, representing an improvement of 54.06%. Meanwhile, the BMSE increases only slightly, demonstrating that the optimization strategy achieves significant gains in drilling efficiency with minimal additional energy consumption.

By repeating the above-described parameter optimization process at different depths of Well A11, a comprehensive drilling parameter optimization scheme for the entire section was developed. The comparisons of WOB, RPM, ROP, and BMSE before and after optimization are shown in Fig. 11. Overall, the optimization results demonstrate varying control strategies and notable improvements in drilling performance across different formations, which can be summarized in two main categories.

(1) Formations with significant improvement in ROP and efficiency (H2 and H3 strata)

The H2 and H3 strata exhibit clear improvements in ROP with minimal change in BMSE, indicating a substantial enhancement in drilling efficiency. Despite the similar performance outcomes, their respective optimization strategies differ significantly. In the H2 strata, both WOB and RPM increased notably after optimization. This suggests that under the prevailing formation conditions, a strategy of simultaneously increasing WOB and RPM is effective for achieving rapid rock breaking. In contrast, the H3 strata shows a considerable increase in WOB, but a slight decrease in RPM. This implies that for this formation, a "high WOB, medium RPM" strategy is more effective in improving drilling efficiency, likely due to formation-specific rock properties and bit–rock interaction dynamics.

(2) Formations with stable ROP and enhanced energy efficiency (H1 and H4 strata)

The H1 and H4 strata exhibit a relatively stable ROP alongside a significant reduction in BMSE, indicating that the optimization process effectively reduced energy consumption while maintaining drilling efficiency. For the H1 strata, the optimal strategy primarily involved reducing WOB and increasing RPM, which led to improved energy efficiency by enhancing the rock-breaking effectiveness with less axial force. In the case of the H4 strata, which is characterized by greater burial depth and more complex geological conditions, the optimal combination of WOB and RPM varies with well depth. Despite these variations, the overall ROP remains stable, while the mechanical energy utilization rate improves markedly, demonstrating the model's ability to adapt to challenging subsurface environments and promote energy-efficient drilling.

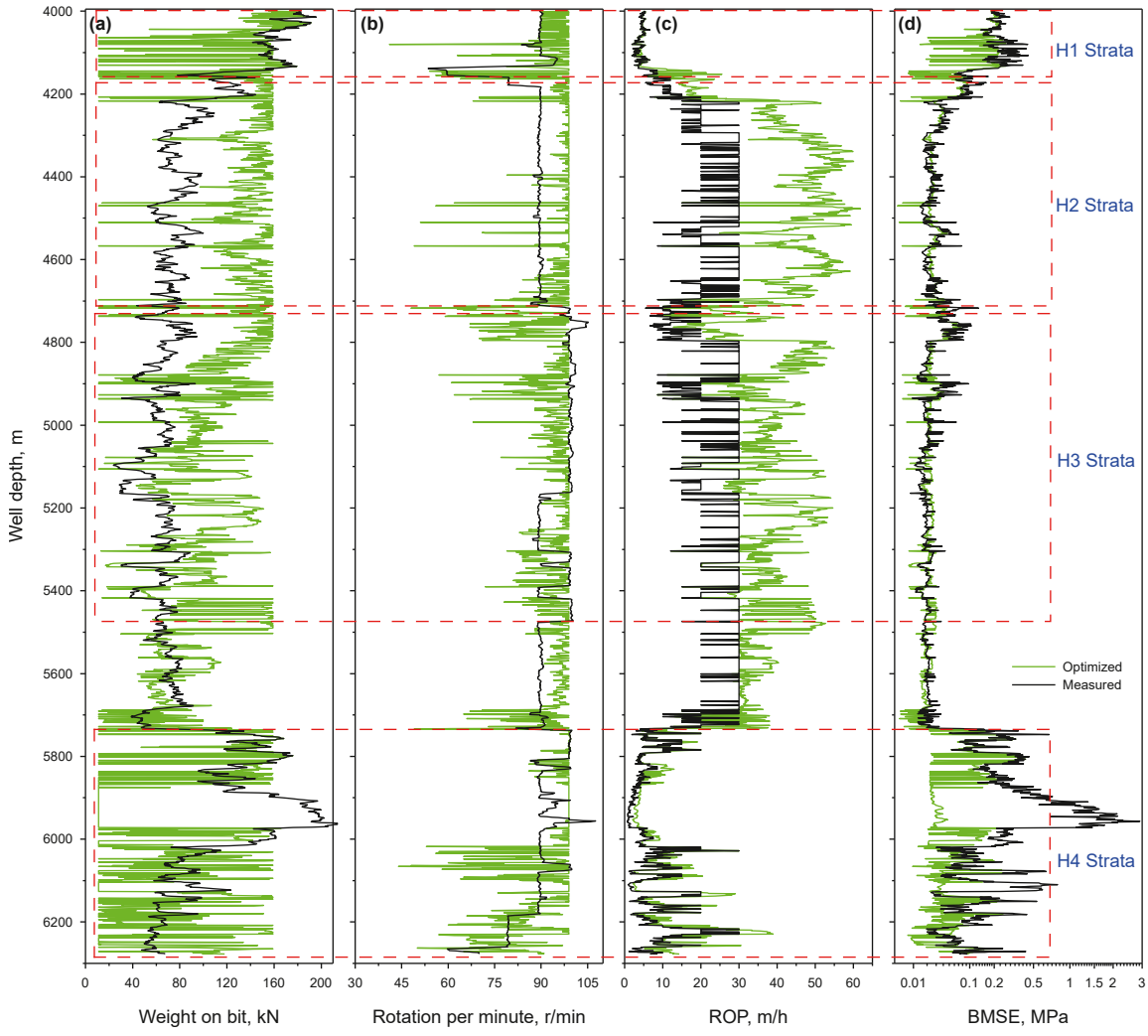


Fig. 11. Comparison of drilling parameters before and after optimization: (**a**) WOB; (**b**) RPM; (**c**) ROP; (**d**) BMSE.

Table 4
Statistical table of control parameters and ROP before and after drilling optimization of Well A11.

Type	Measured				Optimized			
	WOB	RPM	ROP	BMSE	WOB	RPM	ROP	BMSE
Mean	86.49	91.87	19.32	0.12	102.92	94.07	29.19	0.047
Standard deviation	39.23	6.61	10.83	0.27	50.86	8.60	17.13	0.056
Minimum	23.68	53.6	0.64	0.0084	11	41	1.94	0.0037
Maximum	213.8	107.6	30	2.9	191.38	99.8	61.88	0.4223

The statistical analysis of WOB, RPM, ROP, and BMSE for the entire Well A11 before and after optimization is presented in Table 4. Following optimization, the average WOB increased from 86.49 to 102.92 kN (an increase of 18.99%). The average RPM showed a slight increase from 91.87 to 94.07 r/min, remaining essentially stable. In terms of performance indicators, the average ROP rose significantly from 19.32 to 29.19 m/h, representing a 51.09% improvement. Simultaneously, the average BMSE dropped substantially from 0.12 to 0.047 MPa, reflecting a marked reduction in energy consumption.

Overall, these results validate the effectiveness of the proposed drilling parameter optimization strategy. By identifying the optimal combination of WOB and RPM, the strategy successfully achieved the dual objectives of enhancing ROP and reducing energy usage. This demonstrates not only the accuracy and adaptability of the DCDNN-based ROP prediction model, but also its engineering applicability and potential for intelligent optimization in deep and complex drilling environments.

4. Analysis

4.1. Significance of prediction accuracy

To further evaluate the prediction accuracy and generalization capability of the proposed DCDNN model, a conventional data-driven DNN was employed as a baseline for comparison. Both models were trained using identical datasets, preprocessing procedures, and hyperparameter optimization strategies, to ensure a fair comparison.

Fig. 12 presents a comprehensive comparison of the ROP prediction results for the DCDNN and traditional DNN models in the Paleogene Kumugeliemu strata of Well A11. Fig. 12(a) displays the predicted versus measured ROP curves across the entire well section. Overall, the DCDNN model demonstrates a closer fit to the measured data than the traditional DNN model. This advantage is particularly evident in the 4500–6000 m interval, where large fluctuations in ROP occur. In these sections, the DCDNN model achieves notably higher prediction accuracy, reflecting its enhanced ability to learn complex formation-behavior patterns. Fig. 12(b) and (c) provide local comparisons for the 4400–4510 and 5480–5590 m intervals, respectively. In both cases, the DCDNN model more accurately captures the local fluctuation trends and rate changes of the measured ROP. This improved performance can be attributed to the knowledge-driven constraint mechanisms embedded in the DCDNN model, which enhances its ability to generalize across complex geological conditions. In contrast, the traditional DNN model tends to overfit abrupt variations, leading to reduced robustness and poorer predictive reliability when applied to unseen data.

Fig. 12(d) presents the error distribution of the traditional DNN model across the training, validation, and test sets. The MSE values are 0.24, 0.50, and 32.04, respectively, while the MRE values are 5.31%, 7.32%, and 28.09%, respectively. The substantial increase in test set error highlights the DNN model's limited generalization ability when encountering unfamiliar drilling conditions.

As shown in Fig. 12(e) and Table 5, the DCDNN model exhibits slightly higher MRE than the conventional DNN on the training and validation sets. However, this apparent reduction in in-sample fitting accuracy should not be interpreted as inferior model performance. Instead, it reflects the regularization effect induced by the embedded physical constraints within the DCDNN framework. Unlike conventional DNNs, which primarily minimize empirical loss and may overfit local noise or spurious correlations in data-dense regions, the DCDNN introduces domain-specific drilling knowledge in the form of soft correlation constraints and hard boundary constraints. These constraints effectively restrict the hypothesis space to physically admissible solutions, thereby limiting the model's flexibility to fit high-frequency fluctuations or measurement noise present in the training data. As a result, the DCDNN prioritizes physically consistent trends over local error minimization, leading to a modest increase in training and validation errors.

This constraint-guided learning strategy substantially enhances the model's generalization performance. On the test set, which represents previously unseen drilling conditions, the DCDNN achieves a markedly lower MRE of 15.92%, compared to 28.09% for the conventional DNN. The reduction of 12.17 points clearly demonstrates the superior robustness and extrapolation capability of the DCDNN model. This improvement is particularly significant in boundary regions and data-sparse intervals, where purely data-driven models tend to produce unstable or non-physical predictions.

4.2. Effectiveness of physical constraints

Fig. 13 presents the ROP prediction results of the traditional DNN model within the feasible domain of WOB and RPM at a depth of 4953 m in Well A11. Fig. 13(a) illustrates the three-dimensional response surface of the predicted ROP. As can be observed, and in conjunction with the training data distribution shown in Fig. 5, the model produces relatively accurate and reliable predictions within regions well-covered by training data. This indicates that, in data-dense areas, the DNN model can learn meaningful relationships between control parameters and ROP. However, when the control parameters exceed the range represented in the training data, the model's prediction accuracy deteriorates significantly, even producing physically unrealistic results. For instance, in the region of high WOB and high RPM, the model predicts ROP values approaching zero, which is clearly inconsistent with the expected behavior in actual drilling operations. This behavior reveals a fundamental limitation of the traditional DNN model, its lack of generalization capability beyond the training data domain. The two-dimensional contour map in Fig. 13(b) further reinforces this issue. The prediction surface is reasonably smooth and interpretable within the densely sampled parameter regions, but becomes highly distorted and erratic in data-sparse areas. These distortions lead to unreliable predictions and severely limit the model's

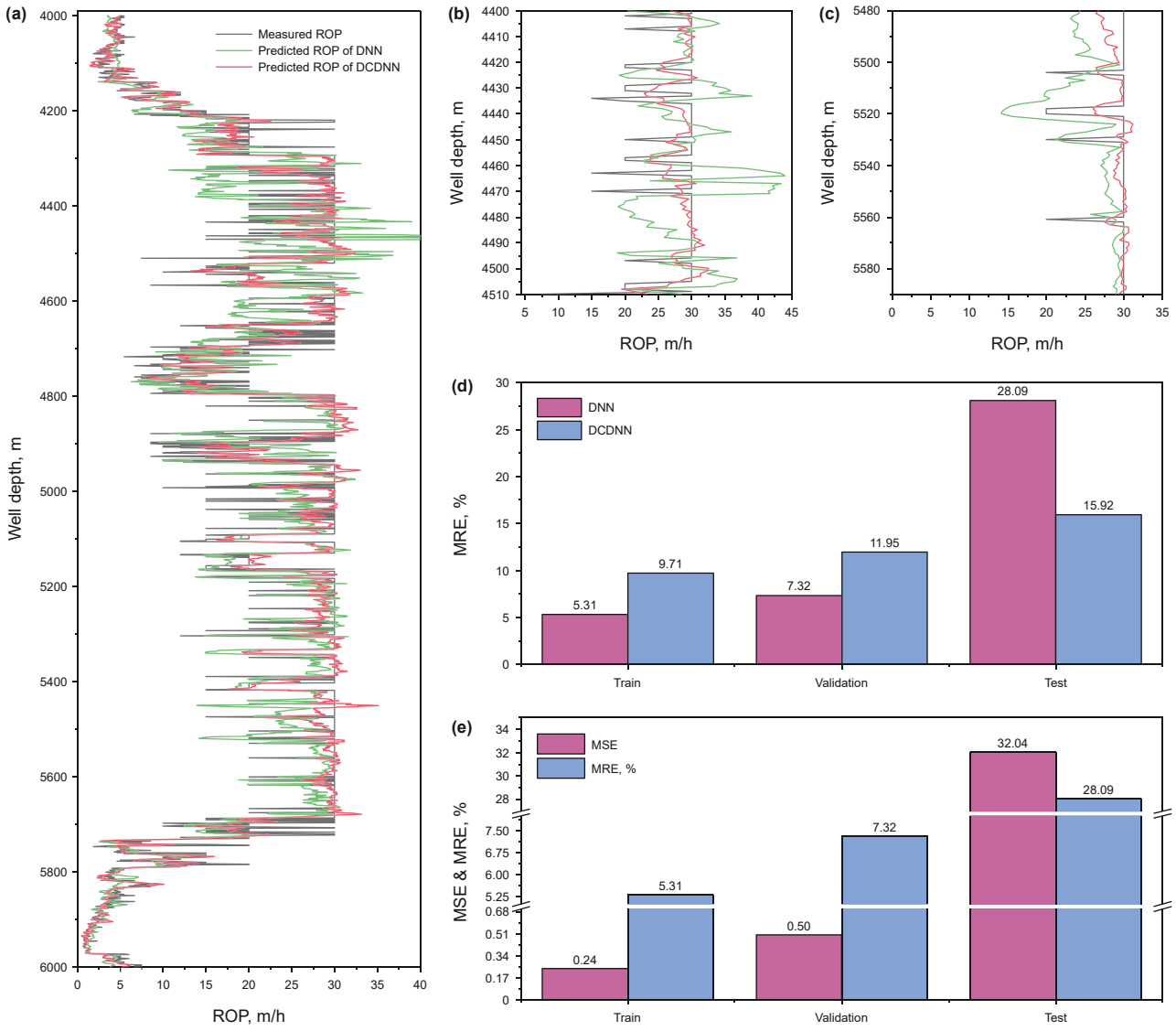


Fig. 12. Comparison of ROP prediction performance between the DCDNN model and the DNN model: (**a**) Comparison of ROP predictions for Well A11; (**b**) local ROP prediction comparison from 4400 to 4510 m; (**c**) local ROP prediction comparison from 5480 to 5590 m; (**d**) performance of the DNN model on the training set, validation set, and test set; (**e**) comparison of MRE between the DNN and DCDNN models.

Table 5
Prediction values and error statistics of the DNN and DCDNN models.

Type		DNN		DCDNN	
		Maximum	Minimum	Maximum	Minimum
Train	ROP	32.08	−0.25	34.01	0.30
	Absolute error, m/h	4.93	0	7.518	0
	Relative error, %	122.65	0	208.46	0
Test	ROP, m/h	44.10	0.98	32.12	0.48
	Absolute error, m/h	28.32	0.003	21.04	0.00048
	Relative error, %	348.73	0.019	302.32	0.0128

applicability in real-world scenarios where operational parameters may vary beyond the historical data range.

However, as evidenced by the results in Fig. 8, even in regions where the training data is relatively sparse, the DCDNN model is still capable of generating smooth and physically consistent predictions of the ROP. The model avoids prediction distortion and does not exhibit non-physical behavior, such as abrupt drops or unrealistic values, which demonstrates its strong generalization ability and robustness. This outcome confirms that the drilling physics knowledge embedded through the integration of soft and hard constraint mechanisms has been effectively incorporated into the model's prediction process. By aligning the learning process with domain-specific physical principles and boundary conditions, the DCDNN model achieves significantly enhanced prediction reliability and engineering adaptability, particularly in boundary regions and low-sample-density intervals, where purely data-driven models often fail. These findings underscore the value of knowledge-informed neural networks in improving the credibility and practical deployment potential of intelligent drilling systems.

Fig. 14 illustrates the response behavior of the DCDNN model and the traditional DNN model to key input parameters during ROP prediction, based on partial dependence plots (PDPs). The PDP method is used to analyze the individual influence of three critical input variables (WOB, RPM, and BF) on the predicted ROP. Fig. 14(a–c) show the influence trends of WOB, RPM, and BF,

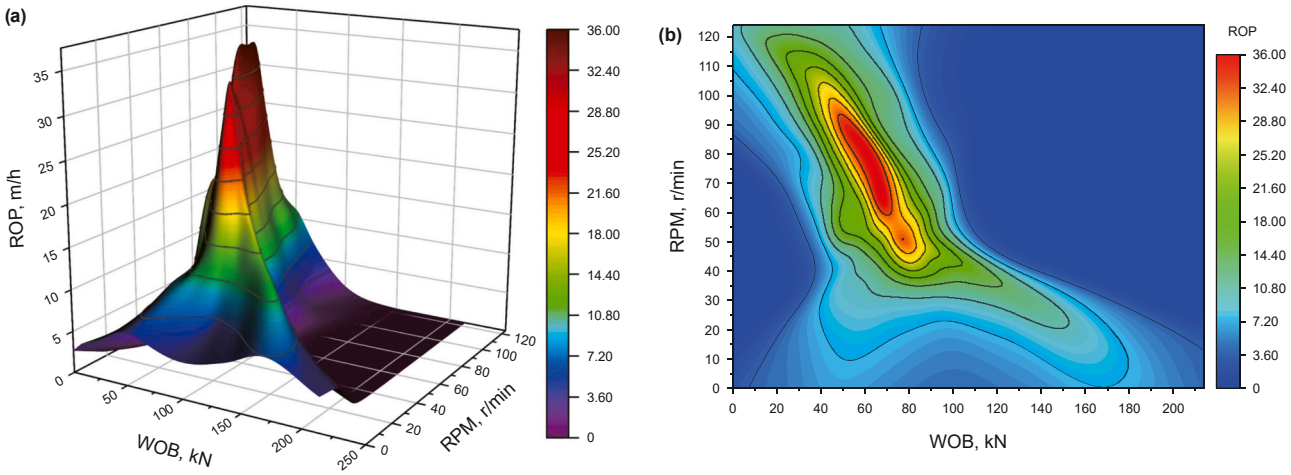


Fig. 13. Distribution of control parameters and ROP of the DNN model at a depth of 4953 m in Well A11: (**a**) Three-dimensional distribution of ROP; (**b**) two-dimensional contour map of the predicted ROP.

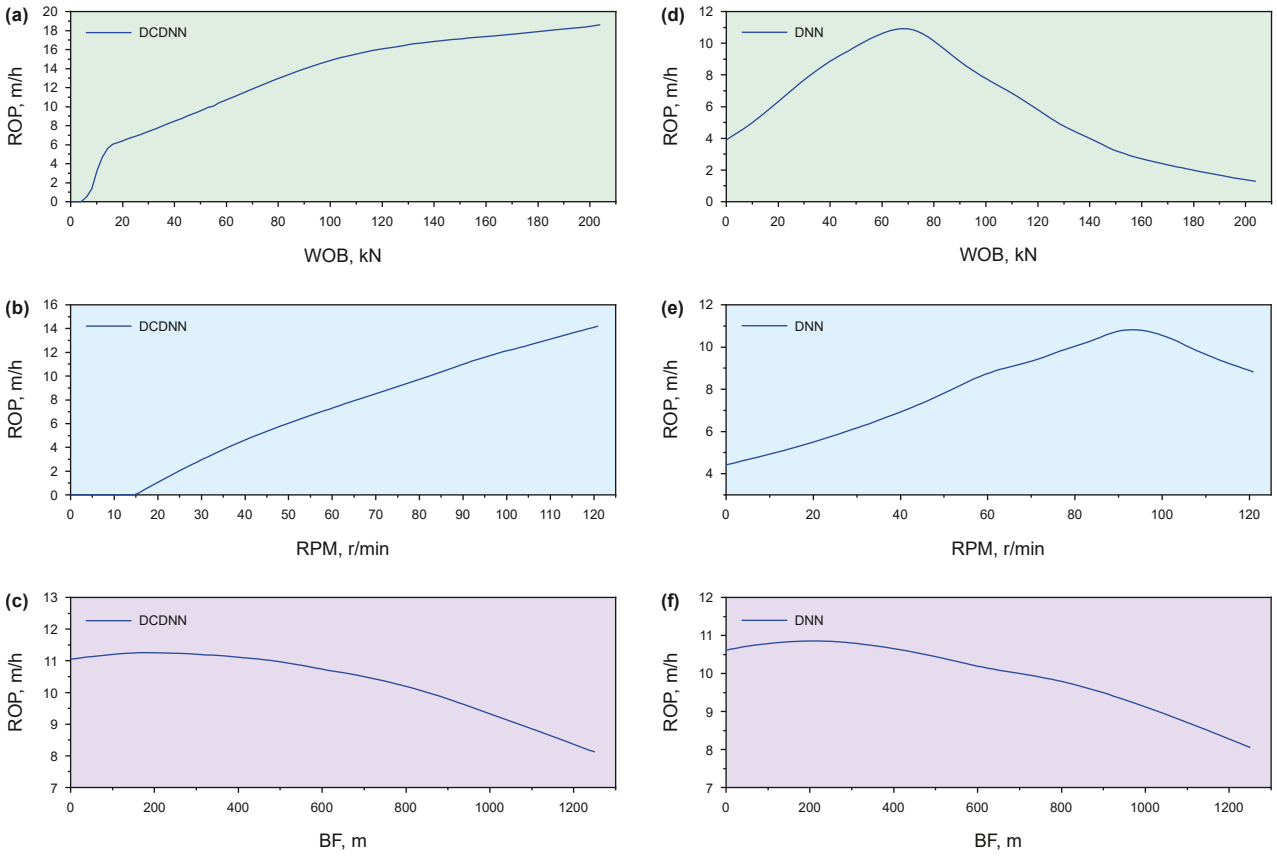


Fig. 14. Partial dependence plots of selected input parameters for the DCDNN and DNN models: (**a**) Effect of WOB on ROP in the DCDNN model; (**b**) effect of RPM on ROP in the DCDNN model; (**c**) effect of BF on ROP in the DCDNN model; (**d**) effect of WOB on ROP in the DNN model; (**e**) effect of RPM on ROP in the DNN model; (**f**) effect of BF on ROP in the DNN model.

respectively, in the DCDNN model, while Fig. 14(d–f) present the corresponding responses in the traditional DNN model.

As shown in Fig. 14(a), the DCDNN model captures the threshold effect of WOB accurately: when WOB is below the threshold, the predicted ROP is zero; once WOB exceeds the threshold, ROP increases monotonically with WOB. This trend aligns well with physical drilling principles, where greater axial force enhances bit–rock interaction, thereby improving penetration efficiency. A similar physically consistent trend is observed in Fig. 13(b). When RPM is below the threshold value, the ROP remains zero; once the threshold is exceeded, increasing RPM leads to a continuous rise in ROP, reflecting the well-established mechanism that higher rotation speed increases the bit's cutting frequency and rock-breaking efficiency. In Fig. 14(c) and (f), the

response curve between BF and ROP exhibits a nonlinear trend, initial increases in BF enhance ROP, reflecting stabilization of the drilling process, but excessive footage is often associated with reduced ROP, which may reflect bit wear effects observed in field operations. This relationship closely mirrors practical drilling observations and reinforces the physical consistency of the DCDNN model.

In contrast, the traditional DNN model displays less physically meaningful behavior. In Fig. 14(d), the WOB-ROP relationship is non-monotonic, first increasing and then decreasing, which contradicts the expected physical trend. Similarly, Fig. 14(e) shows a fluctuating and irregular response of ROP to RPM, lacking the expected threshold behavior and monotonicity. These inconsistencies indicate that, in the absence of embedded domain knowledge, the DNN model is more susceptible to overfitting, particularly in boundary or data-sparse regions.

These findings demonstrate that the DCDNN model (by incorporating soft constraints and hard constraints) provides physically consistent, interpretable, and robust predictions. This integration of prior domain knowledge significantly enhances the credibility, stability, and engineering applicability of intelligent ROP prediction, offering a more trustworthy foundation for downstream optimization and decision-making.

Table 5 presents the predicted values and error statistics of the ROP for both the traditional DNN model and the proposed DCDNN model on the training set and test set.

In the training set, the predicted ROP range of the DCDNN model is 0.30–34.01 m/h, fully conforming to the physical constraint that ROP must be non-negative. In contrast, the DNN model predicts a minimum ROP of −0.25 m/h, a physically unrealistic value, revealing the model's lack of effective boundary constraint mechanisms. Regarding error statistics in the training set, the DNN model exhibits a maximum absolute error of 4.93 m/h and a maximum relative error of 122.65%. While the DCDNN model's maximum absolute error is slightly higher at 7.52 m/h, its maximum relative error reaches 208.46%. This phenomenon arises because the soft constraints and hard constraints restrict the feasible solution space, preventing the model from overfitting near physical boundary regions. As a result, local errors may increase at certain boundary-adjacent samples. However, this restriction simultaneously suppresses extreme residual fluctuations, reduces overall residual variance, and strengthens physical consistency. Statistical analysis demonstrates that, compared with the deep neural network, the deep constrained dual neural network exhibits a 27% reduction in residual variance despite the increase in training error. This indicates that the constrained model incurs a moderate increase in bias while achieving a significant reduction in variance, which is consistent with the theoretical expectations of constrained optimization under physics-informed regularization.

In the test set, the DCDNN model produces a maximum predicted ROP of 32.12 m/h, compared to 44.10 m/h in the DNN model. This indicates that the DCDNN model adopts a more conservative estimation strategy in high ROP regions, effectively mitigating the risk of extrapolation error in unseen parameter ranges. Furthermore, the DCDNN model demonstrates clear improvements in error performance: its maximum absolute error is 21.04 m/h, representing a 25.7% reduction compared to the DNN model (28.32 m/h); the maximum relative error is reduced from 348.74% in the DNN model to 302.32%, a 13.3% improvement. These results highlight the enhanced generalization capability and physical reliability of the DCDNN model, especially in complex or underrepresented parameter spaces.

5. Conclusions

This work presents a drilling knowledge-constrained deep neural network (DCDNN) model that integrates domain-specific drilling knowledge with deep learning techniques to predict the ROP in ultra-deep drilling environments. By incorporating critical physical constraints such as weight on bit (WOB), revolutions per minute (RPM), and bit footage (BF), the model ensures both physical consistency and improved accuracy in predictions, making it a significant advancement over traditional data-driven models. The DCDNN model was validated using field data from seven ultra-deep wells in the Tarim Oilfield, China. The results demonstrate that the DCDNN model outperforms conventional deep neural networks in both prediction accuracy and generalization ability. Specifically, the mean relative error (MRE) for the DCDNN model on the test set was 15.92%, compared to 28.09% for the traditional DNN model. This reduction in MRE demonstrates DCDNN's superior ability to generalize across unseen data, particularly in boundary regions where training data is sparse. Furthermore, the MSE of the DCDNN on the test set was 10.84, significantly lower than the 28.32 mean squared error (MSE) value of the DNN model, highlighting the enhanced prediction accuracy of the DCDNN. The conventional DNN model also produced physically unrealistic predictions, such as a minimum ROP of −0.25 m/h, which is physically impossible, while the DCDNN model maintained physically consistent predictions with a ROP range of 0.30–34.01 m/h. In addition, the drilling parameter optimization method ensures the selection of the optimal drilling strategy in different formations. The average ROP of the test wells is projected to increase substantially from 19.32 to 29.19 m/h, while the average bit mechanical specific energy (BMSE) is projected to decrease markedly from 0.12 to 0.047 MPa.

In summary, the DCDNN model provides a promising solution for integrating drilling physics with deep learning. It improves the accuracy of ROP prediction, optimizes drilling parameters for enhanced efficiency, and reduces energy consumption. This model offers significant theoretical innovation and practical engineering value, laying a foundation for the future development of intelligent drilling technologies in deep and complex formations.

Future studies can further improve the DCDNN by integrating more advanced constraints and multi-fidelity data sources. Expanding the model's application to other challenging geological environments and sectors, such as geothermal energy and carbon capture, could further highlight its versatility and cross-disciplinary benefits.

CRediT authorship contribution statement

Zhi-Jun Pei: Writing – original draft, Investigation, Data curation. **Xian-Zhi Song:** Writing – review & editing, Supervision. **Bo Feng:** Writing – original draft, Methodology. **Jian He:** Resources, Methodology, Investigation. **Shou-Ceng Tian:** Writing – review & editing, Writing – original draft, Methodology, Investigation, Data curation. **Gen-Sheng Li:** Writing – review & editing, Validation, Supervision, Methodology.

Declaration of competing interest

The authors declare that they have no known competing financial interests or personal relationships that could have appeared to influence the work reported in this paper.

Acknowledgments

The authors greatly thanked the financial support from the National Science Fund for Distinguished Young Scholars (funded by National Natural Science Foundation of China, No. 52125401), the Postdoctoral Fellowship Program of CPSF under Grant Number GZC20251947 and China National Petroleum Corporation-Southwest Petroleum University Innovation Consortium supports the development of interdisciplinary disciplines "Unveiling the Challenges and Leading the Team" project (Funding No. 2024CXJB03).

References

Alsaihati, A., Elkatatny, S., Gamal, H., 2022. Rate of penetration prediction while drilling vertical complex lithology using an ensemble learning model. J. Petrol. Sci. Eng. 208, 109335. https://doi.org/10.1016/j.petrol.2021.109335.

Barbosa, L.F.F.M., Nascimento, A., Mathias, M.H., et al., 2019. Machine learning methods applied to drilling rate of penetration prediction and optimization - a review. J. Petrol. Sci. Eng. 183, 106332. https://doi.org/10.1016/j.petrol.2019.106332.

Beucler, T., Pritchard, M., Rasp, S., et al., 2021. Enforcing analytic constraints in neural networks emulating physical systems. Phys. Rev. Lett. 126 (9), 098302. https://doi.org/10.1103/physrevlett.126.098302.

Chen, Y., Huang, D., Zhang, D., et al., 2021. Theory-guided hard constraint projection (HCP): A knowledge-based data-driven scientific machine learning method. J. Comput. Phys. 445, 110624. https://doi.org/10.1016/j.jcp.2021.110624.

Elmgerbi, A.M., Ettinger, C.P., Tekum, P.M., et al., 2021. Application of machine learning techniques for real time rate of penetration optimization. In: SPE/IADC Middle East Drilling Technology Conference and Exhibition. https://doi.org/10.2118/202184-ms .

Feng, Z., Gani, H., Damayanti, A.D., et al., 2023. An explainable ensemble machine learning model to elucidate the influential drilling parameters based on rate of penetration prediction. Geoenergy Sci. Eng. 231, 212231. https://doi.org/10.1016/j.geoen.2023.212231.

Gan, C., Cao, W.H., Liu, K.Z., et al., 2022. A novel dynamic model for the online prediction of rate of penetration and its industrial application to a drilling process. J. Process Control 109, 83–92. https://doi.org/10.1016/j.jprocont.2021.12.002.

Gupta, R., Bhui, U.K., 2025. Transforming oil well drilling: prediction of real-time rate of penetration with novel machine learning approach in varied lithological formations. J. Energy Resour. Technol., Part B: Subsurface Energy and Carbon Capture 1 (1), 011003. https://doi.org/10.1115/1.4066015.

Hegde, C., Daigle, H., Millwater, H., et al., 2017. Analysis of rate of penetration (ROP) prediction in drilling using physics-based and data-driven models. J. Pet. Sci. Eng. 159, 295–306. https://doi.org/10.1016/j.petrol.2017.09.020.

Höhn, P., Odebrett, F., Shahid, K., et al., 2022. Framework for automated generation of real-time rate of penetration models. J. Petrol. Sci. Eng. 213, 110369. https://doi.org/10.1016/j.petrol.2022.110369.

Huang, Z., Zhu, L., Wang, C.C., et al., 2024. Intelligent prediction of rate of penetration using mechanism-data fusion and transfer learning. Processes 12 (10), 2133. https://doi.org/10.3390/pr12102133.

Jagtap, A.D., Kawaguchi, K., Karniadakis, G.E., 2020. Adaptive activation functions accelerate convergence in deep and physics-informed neural networks. J. Comput. Phys. 404, 109136. https://doi.org/10.1016/j.jcp.2019.109136.

Jalakani, R., Tabatabaee Moradi, S.S., 2024. Rate of penetration prediction with uncertainty assessment: case study of a middle-east oil field. Results Eng. 21, 101793. https://doi.org/10.1016/j.rineng.2024.101793.

Jiao, S., Li, W., Li, Z., et al., 2024. Hybrid physics-machine learning models for predicting rate of penetration in the halahatang oil field, Tarim Basin. Sci. Rep. 14 (1), 5957. https://doi.org/10.1038/s41598-024-56640-y.

Li, G., Song, X., Tian, S., et al., 2022. Intelligent drilling and completion: A review. Engineering 18, 33–48. https://doi.org/10.1016/j.eng.2022.07.014.

Lu, L., Pestourie, R., Yao, W., et al., 2021. Physics-informed neural networks with hard constraints for inverse design. SIAM J. Sci. Comput. 43 (6), B1105–B1132. https://doi.org/10.1137/21m1397908.

Ma, Z., Hsu, M., Hu, H., et al., 2024. Hybrid strategies for interpretability of rate of penetration prediction: automated machine learning and SHAP interpretation. In: 58th U.S. Rock Mechanics/Geomechanics Symposium. https://doi.org/10.56952/arma-2024-0315.

Mahmoodzadeh, A., Nejati, H.R., Mohammadi, M., et al., 2022. Forecasting tunnel boring machine penetration rate using LSTM deep neural network optimized by grey wolf optimization algorithm. Expert Syst. Appl. 209, 118303. https://doi.org/10.1016/j.eswa.2022.118303.

Maurer, W.C., 1962. The "perfect-cleaning" theory of rotary drilling. J. Petrol. Technol. 14 (11), 1270–1274. https://doi.org/10.2118/408-pa.

Mazen, A.Z., Rahmanian, N., Mujtaba, I., et al., 2021. Prediction of penetration rate for PDC bits using indices of rock drillability, cuttings removal, and bit wear. SPE Drill. Complet 36 (2), 320–337. https://doi.org/10.2118/204231-pa.

Mohan, A.T., et al., 2020. Embedding hard physical constraints in neural network coarse-graining of 3D turbulence. arXiv preprint arXiv:2002, 00021.

Pei, Z.J., Song, X.Z., Wang, H.T., et al., 2024a. Interpretation and characterization of rate of penetration intelligent prediction model. Pet. Sci. 21 (1), 582–596. https://doi.org/10.1016/j.petsci.2023.10.011.

Pei, Z., Song, X., Hu, Z., et al., 2024b. Intelligent optimization of drilling parameters based on multiple drilling agents. In: International Petroleum Technology Conference. https://doi.org/10.2523/iptc-24457-ms.

Pei, Z., Song, X., Ji, Y., et al., 2023. Wide and deep cross network for the rate of penetration prediction. Geoenergy Sci. Eng. 229, 212066. https://doi.org/10.1016/j.geoen.2023.212066.

Raissi, M., Perdikaris, P., Karniadakis, G.E., et al., 2019. Physics-informed neural networks: A deep learning framework for solving forward and inverse problems involving nonlinear partial differential equations. J. Comput. Phys. 378, 686–707. https://doi.org/10.1016/j.jcp.2018.10.045.

Ren, C., Huang, W., Gao, D., et al., 2023. Predicting rate of penetration of horizontal drilling by combining physical model with machine learning method in the China Jimusar Oil Field. SPE J. 28 (6), 2713–2736. https://doi.org/10.2118/212294-pa.

Safarov, A., Iskandarov, V., Solomonov, D., 2022. Application of machine learning techniques for rate of penetration prediction. In: SPE Annual Caspian Technical Conference. https://doi.org/10.2118/212088-ms.

Sheng, H., Yang, C., 2021. PFNN: a penalty-free neural network method for solving a class of second-order boundary-value problems on complex geometries. J. Comput. Phys. 428, 110085. https://doi.org/10.1016/j.jcp.2020.110085.

Shimodaira, H., 2000. Improving predictive inference under covariate shift by weighting the log-likelihood function. J. Stat. Plann. Inference 90 (2), 227–244. https://doi.org/10.1016/S0378-3758(00)00115-4.

Soares, C., Armenta, M., Panchal, N., 2020. Enhancing reamer drilling performance in deepwater gulf of Mexico wells. SPE Drill. Complet 35 (3), 329–356. https://doi.org/10.2118/200480-pa.

Waughman, R.J., Kenner, J.V., Moore, R.A., 2002. Real-time specific energy monitoring reveals drilling inefficiency and enhances the understanding of when to pull worn PDC bits. In: IADC/SPE Drilling Conference. https://doi.org/10.2118/74520-ms.

Xu, K., Darve, E., 2022. Physics constrained learning for data-driven inverse modeling from sparse observations. J. Comput. Phys. 453, 110938. https://doi.org/10.1016/j.jcp.2021.110938.

Yang, J., Wang, J., Jin, F., et al., 2025. A physics informed convolution neural network for spatiotemporal temperature analysis of concrete dams. Eng. Appl. Artif. Intell. 150, 110624. https://doi.org/10.1016/j.engappai.2025.110624.

Yang, L., Meng, X., Karniadakis, G.E., 2021. B-PINNs: Bayesian physics-informed neural networks for forward and inverse PDE problems with noisy data. J. Comput. Phys. 425, 109913. https://doi.org/10.1016/j.jcp.2020.109913.

Yang, Y., Perdikaris, P., 2019. Adversarial uncertainty quantification in physics-informed neural networks. J. Comput. Phys. 394, 136–152. https://doi.org/10.1016/j.jcp.2019.05.027.

Young Jr., F.S., 1969. Computerized drilling control. J. Petrol. Technol. 21 (4), 483–496. https://doi.org/10.2118/2241-pa.

Yuan, Q., He, M., Chen, Z., et al., 2025. A real-time prediction method for rate of penetration sequence in offshore deep wells drilling based on attention mechanism-enhanced BiLSTM model. Ocean Eng. 325, 120820. https://doi.org/10.1016/j.oceaneng.2025.120820.

Zadrozny, B., 2004. Learning and evaluating classifiers under sample selection bias. In: Proceedings of the Twenty-First International Conference on Machine Learning, p. 114. https://doi.org/10.1145/1015330.1015425.

Zhang, C., Song, X., Liu, Z., et al., 2023. Real-time and multi-objective optimization of rate-of-penetration using machine learning methods. Geoenergy Sci. Eng. 223, 211568. https://doi.org/10.1016/j.geoen.2023.211568.

Zhang, D., Lu, L., Guo, L., et al., 2019. Quantifying total uncertainty in physics-informed neural networks for solving forward and inverse stochastic problems. J. Comput. Phys. 397, 108850. https://doi.org/10.1016/j.jcp.2019.07.048.

Zhao, Y., Noorbakhsh, A., Koopialipoor, M., et al., 2020. A new methodology for optimization and prediction of rate of penetration during drilling operations. Eng. Comput. 36 (2), 587–595. https://doi.org/10.1007/s00366-019-00715-2.

Zhou, F., Fan, H., Liu, Y., et al., 2022. Application of XGBoost algorithm in rate of penetration prediction with accuracy. In: International Petroleum Technology Conference. https://doi.org/10.2523/iptc-22100-ms.

Zhou, F., Fan, H., Liu, Y., et al., 2023. Hybrid model of machine learning method and empirical method for rate of penetration prediction based on data similarity. Appl. Sci. 13 (10), 5870. https://doi.org/10.3390/app13105870.